Cell Reports

Article

LXR stimulates a metabolic switch and reveals cholesterol homeostasis as a statin target in Tasmanian devil facial tumor disease

Graphical Abstract

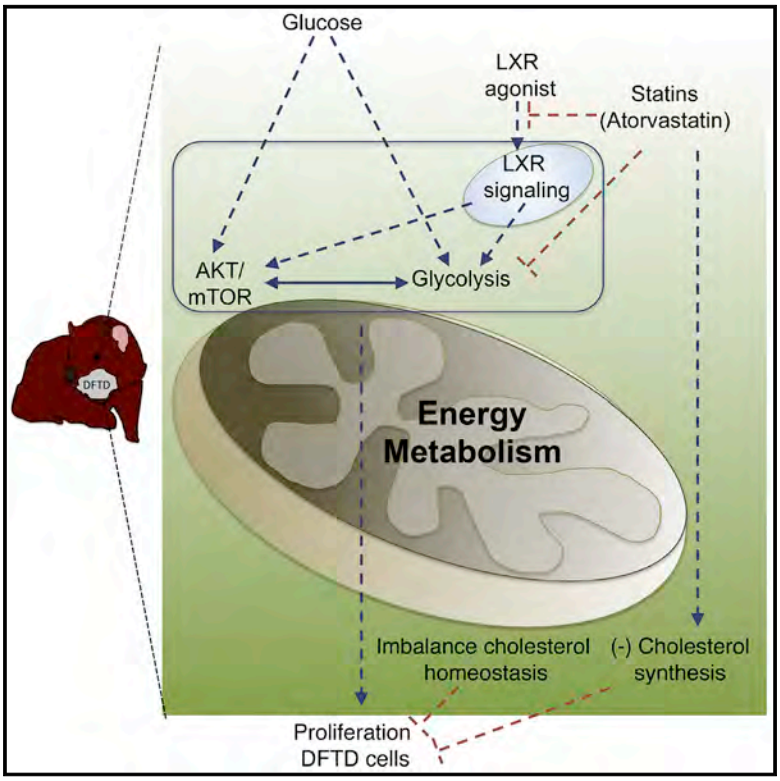

Highlights

- Liver-X nuclear receptor-β signaling enhances the proliferation of DFTD cells
- DFTD cells depend on carbohydrate metabolism to proliferate
- Maintaining cholesterol homeostasis is essential for the proliferation of DFTD cells
- Atorvastatin constitutes a feasible treatment against DFTD-infected animals

Authors

Maria P. Ikonomopoulou,
Yaiza Lopez-Mancheño,
Marta G. Novelle, ...,
Pablo Jose Fernandez-Marcos,
Grant A. Ramm,
Manuel Alejandro Fernandez-Rojo

Correspondence

maria.ikonomopoulou@imdea.org (M.P.I.),
manuel.fernandez@imdea.org (M.A.F.-R.)

In brief

Devil facial tumor disease (DFTD) threatens the Tasmanian devil with extinction. Ikonomopoulou et al. investigate how the energy metabolism of DFTD cells drives tumor growth. Using *in vitro* and *in vivo* models, they characterize the impact of cholesterol homeostasis imbalance in the integrity and proliferation of DFTD cells and tumors.

Ikonomopoulou et al., 2021, Cell Reports *34*, 108851
March 16, 2021
https://doi.org/10.1016/j.celrep.2021.108851

CellPress

Cell Reports

CellPress
OPEN ACCESS

Article

LXR stimulates a metabolic switch and reveals cholesterol homeostasis as a statin target in Tasmanian devil facial tumor disease

Maria P. Ikonomopoulou,[1,2,3,8,*] Yaiza Lopez-Mancheño,[4] Marta G. Novelle,[4] Maite Martinez-Uña,[4] Lahiru Gangoda,[6,7] Martin Pal,[6,7] Luis Filipe Costa-Machado,[5] Pablo Jose Fernandez-Marcos,[5] Grant A. Ramm,[1,2] and Manuel Alejandro Fernandez-Rojo[1,2,4,8,9,*]

[1]QIMR Berghofer Medical Research Institute, Brisbane, QLD, Australia
[2]The University of Queensland, Brisbane, QLD, Australia
[3]Translational Venomics Laboratory, Madrid Institute for Advanced Studies (IMDEA) Food, Madrid 28049, Spain
[4]Hepatic Regenerative Medicine Laboratory, Madrid Institute for Advanced Studies (IMDEA) Food, Madrid 28049, Spain
[5]Metabolic Syndrome Laboratory, Madrid Institute for Advanced Studies (IMDEA) Food, Madrid 28049, Spain
[6]Walter and Eliza Hall Institute of Medical Research, 1G Royal Parade, Parkville, Melbourne, VIC 3052, Australia
[7]Department of Medical Biology, The University of Melbourne, Parkville, Melbourne, VIC 3052, Australia
[8]These authors contributed equally
[9]Lead contact
*Correspondence: maria.ikonomopoulou@imdea.org (M.P.I.), manuel.fernandez@imdea.org (M.A.F.-R.)
https://doi.org/10.1016/j.celrep.2021.108851

SUMMARY

Devil facial tumor disease (DFTD) and its lack of available therapies are propelling the Tasmanian devil population toward extinction. This study demonstrates that cholesterol homeostasis and carbohydrate energy metabolism sustain the proliferation of DFTD cells in a cell-type-dependent manner. In addition, we show that the liver-X nuclear receptor-β (LXRβ), a major cholesterol cellular sensor, and its natural ligand 24S-hydroxycholesterol promote the proliferation of DFTD cells via a metabolic switch toward aerobic glycolysis. As a proof of concept of the role of cholesterol homeostasis on DFTD proliferation, we show that atorvastatin, an FDA-approved statin-drug subtype used against human cardiovascular diseases that inhibits cholesterol synthesis, shuts down DFTD energy metabolism and prevents tumor growth in an *in vivo* DFTD-xenograft model. In conclusion, we show that intervention against cholesterol homeostasis and carbohydrate-dependent energy metabolism by atorvastatin constitutes a feasible biochemical treatment against DFTD, which may assist in the conservation of the Tasmanian devil.

INTRODUCTION

The Tasmanian devil (*Sarcophilus harrisii*) is the largest extant carnivorous marsupial (McCallum et al., 2009), distributed on the island state of Tasmania in Australia. However, the Tasmanian devil is an endangered Australian species (McCallum et al., 2009), threatened with extinction within the next 15–25 years because of a contagious and transmissible parasitic form of cancer known as devil facial tumor disease (DFTD) (Wei et al., 2006), which has killed approximately 80% of the species since emerging in 1996 in northeastern Tasmania (McCallum et al., 2009; Pyecroft et al., 2007). Primary DFTD tumors appear on the face or inside the mouth and develop into large globular tumors that metastasize in a short period to internal organs and spread among individuals by biting during mating and territorial fighting (Pearse and Swift, 2006). DFTD causes devil death within 3–6 months of the first appearance of clinical symptoms (Pyecroft et al., 2007).

With no treatment available against DFTD, scientists keep captive, disease-free breeding populations that are released into the wild to maintain the species. Major research efforts are focused on understanding the genetic mutations and the molecular mechanisms underlying the dramatic downregulation of the expression of major histocompatibility complex (MHC) class I that could explain how the DFTD tumor cells proliferate and fail to stimulate the immune system in the Tasmanian devil (Brown et al., 2016; Flies et al., 2016; Patchett et al., 2016; Siddle and Kaufman, 2013; Siddle et al., 2013). An immense step forward has been the characterization of the crosstalk between the receptor tyrosine kinases ERBB and signal transducer and activator of transcription-3 (STAT3) as potential targets to stimulate the immune response in devils (Kosack et al., 2019). However, therapeutic approaches using human chemotherapeutic agents, such as vincristine, doxorubicin, and carboplatin, on DFTD-positive devils have proven unsuccessful (Phalen et al., 2013, 2015). Only recently, the immunomodulatory molecule imiquimod and the gomesin spider peptide have been shown to display apoptotic activity against DFTD cells and with minimum cytotoxicity on healthy devil fibroblasts (FIBs) (Fernandez-Rojo et al., 2018; Patchett et al., 2016). Most

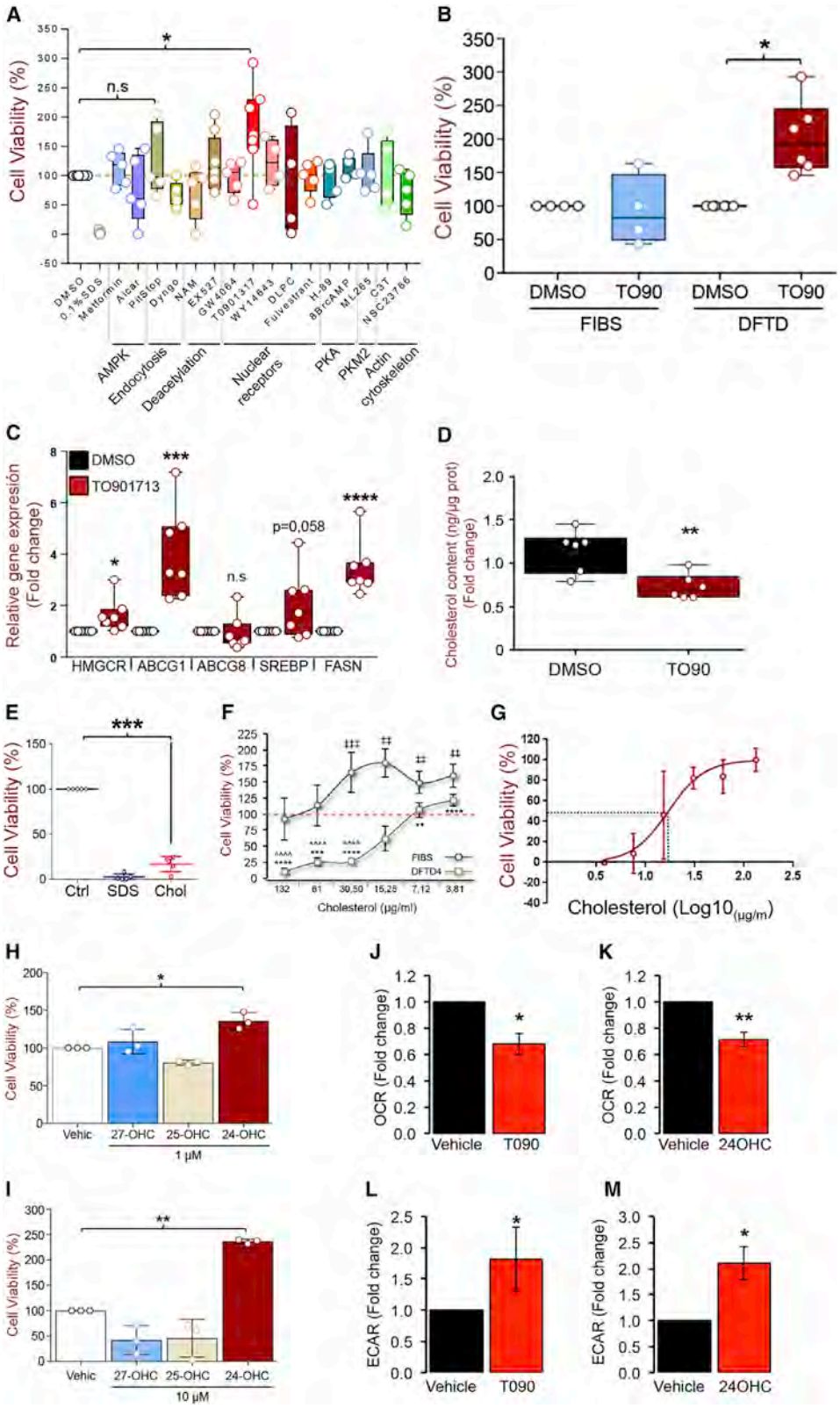

(legend on next page)

molecular mechanisms that drive the proliferation of DFTD cells remain obscure. In this study, we identify cholesterol homeostasis as an essential factor sustaining the proliferation of DFTD cells in a cell-type-dependent manner. Accordingly, we reveal that (1) the liver-X nuclear receptor (LXR) and its natural ligand 24S-hydroxycholesterol (24-OHC) drive the proliferation of DFTD in a cell-type-dependent manner; (2) both LXR and 24-OHC unmasked that DFTD cells rely on carbohydrate metabolism and the Warburg effect like human cancer cells; (3) cholesterol homeostasis is essential for maintaining the proliferative capacity of DFTD cells; and (4) this study provides an intervention via the use of statins as a potential therapeutic approach to reduce DFTD progression *in vivo* using xenograft tumors in nude mice that may contribute to the long-term conservation of Tasmanian devils.

RESULTS

LXR signaling promotes DFTD cell proliferation

Genetic studies have started to dissect the origin and nature of DFTD tumors (Murchison et al., 2010, 2012). However, the lack of detailed insight into the molecular pathways that sustain the proliferation and metastasis of DFTD cells in devil tissues restricts the development of biochemical therapies against this fatal disease. This is hindered by the virtual absence of specific molecular tools and specific markers that permit the molecular characterization of the devil cells. To address this issue and gain further insight into the signaling cascades driving the proliferation of DFTD cells, we performed an unbiased analysis of the effects of available commercial drugs targeting specific signaling pathways (i.e., AMPK, deacetylases, nuclear receptors, and PKA) and cellular processes (i.e., endocytosis and actin re-organization) (Table S1) on the proliferation of the immortalized DFTD4 cell line. Among all drugs tested, we observed that *LXR* agonist T0901317 exacerbates the proliferation and viability of cultured DFTD cells (Figure 1A), but not on the immortalized Tasmanian devil non-transformed skin FIBs (Figure 1B). These results on DFTD4 were recapitulated in two independent DFTD cell lines (DFTD1 and DFTD2) (Figures S1A and S1B). With LXRs acting as cholesterol sensors (Duval et al., 2006; Peet et al., 1998; Repa and Mangelsdorf, 2000, 2002; Venkateswaran et al., 2000; Zelcer et al., 2009), T0901317 stimulated the expression of bona fide LXR target genes, including the cholesterol transporter of the ATP-binding Cassette family ABCG1, the transcription factor SREBP, and the fatty acid synthase (FASN) genes in DFTD cells and in FIBs (Figure 1C; Figure S1C), as well as reduction in the total cholesterol content in the DFTD4 cells (Figure 1D). T0901317 is an agonist of other nuclear receptors, including FXRα, RORα, and ERα at relatively high concentrations of 5 μM. However, T0901317 stimulated the proliferation of DFTD cells at 2.5 and 1.25 μM while exhibiting a trend at 0.625 μM (p value = 0.068) (Figure S1D). In addition, the FXRα agonist GW4064 (Figure 1A), the RORα agonist SR1078 (10 μM), or the ERα agonist estradiol (10 μM) did not promote proliferation in DFTD4 cells (data not shown). Altogether, these data support the proposal that the mode of action of T0901317 is directly through the activation of LXR. We postulated that T0901317- and LXR-induced stimulation of the proliferation of DFTD cells would depend on the cellular cholesterol homeostasis. Supporting this, cell overloading with exogenous cholesterol impaired the growth of DFTD cells (Figure 1E; Figures S1E and S1F), with a half maximal effective concentration (EC_{50}) of 17.01 μg/mL in DFTD4 cells (Figures 1F and 1G). Interestingly, activation of estrogen receptor and cholesterogenesis (Wang et al., 2006) via fulvestrant (Figure 1A) and via the ERα agonist estradiol (10 μM) (data not shown) did not affect DFTD4 growth, suggesting that DFTD4 cells may exhibit a threshold to tolerate certain increases in cholesterol content. Moreover, because agonist-induced activation of other nuclear receptors that mediate reverse cholesterol transport and cholesterol catabolism into bile acids such as LRH-1 (Schoonjans et al., 2002) via DLPC and FXRα (Xu et al., 2016) via GW4064 (Figure 1A) did not promote the proliferation of DFTD4 cells, our results suggest that LXR may specifically drive DFTD proliferation by modulating cholesterol content rather than promoting cholesterol metabolism. Conversely, and unlike in DFTD, cholesterol overloading significantly increased FIB growth at concentrations ranging from 30.50 to 3.81 μg/mL (Figure 1F), supporting cell-type-specific roles of cholesterol in the proliferation of devil cells. The natural ligands mediating LXR activation are 24-OHC, 25S-hydroxycholesterol

Figure 1. LXR activation and the oxysterol 24-OHC promote DFTD proliferation

(A) Drug screening to assess cell proliferation after 48 h of exposure in DFTD4 cells using an MTT assay. Dimethyl sulfoxide (DMSO) was used as the vehicle control, and 0.1% sodium dodecyl sulfate (SDS) was used as the positive control, causing 100% toxicity. Five independent experiments were performed in duplicate.

(B) Liver-X nuclear receptor (LXR) agonist T0901317 (T090) shows cell-specific stimulation in DFTD4 cells and compared with healthy non-transformed skin fibroblasts (FIBs). Four independent experiments were performed in duplicate.

(C) Relative gene expression analysis of LXR target genes. Three independent experiments were performed in duplicate.

(D) Cholesterol content in T090-treated DFTD4 cells in comparison to vehicle (DMSO). Five independent experiments were performed in duplicate.

(E) Effect of exogenous cholesterol (120 μg/mL) on DFTD4 cell proliferation. Five independent experiments were performed in three replicates.

(F) Dose-dependent effect of cholesterol on cell proliferation in DFTD4 cells in comparison to FIBs. Five independent experiments were performed in three replicates.

(G) Cell viability of DFTD4 cells treated with a range of cholesterol concentrations showing the EC_{50} (log 10 scale).

(H and I) Cell proliferation of oxysterols 24-OHC, 25-OHC, and 27-OHC versus untreated cells at 1 μM (H) and 10 μM (I). Three independent experiments were performed in three replicates.

(J and K) Mitochondrial respiration (oxygen consumption rate [OCR]) in (J) T090-treated and (K) 24-OHC-treated DFTD4 cells in comparison to vehicle (DMSO and ethanol, respectively), represented as fold change of picomoles per minute.

(L and M) Glycolytic flux (extracellular acidification rate [ECAR]) in (L) T090-treated and (M) 24-OHC-treated DFTD4 cells in comparison to vehicle (DMSO and ethanol, respectively), represented as fold change of milli-pH per minute.

For OCR and ECAR, five independent experiments were performed in five replicates. DMSO was used as vehicle control in all assays unless reported otherwise. Data are shown as mean ± SEM. *p < 0.05, **p < 0.01, ***p < 0.001, ****p < 0.0001.

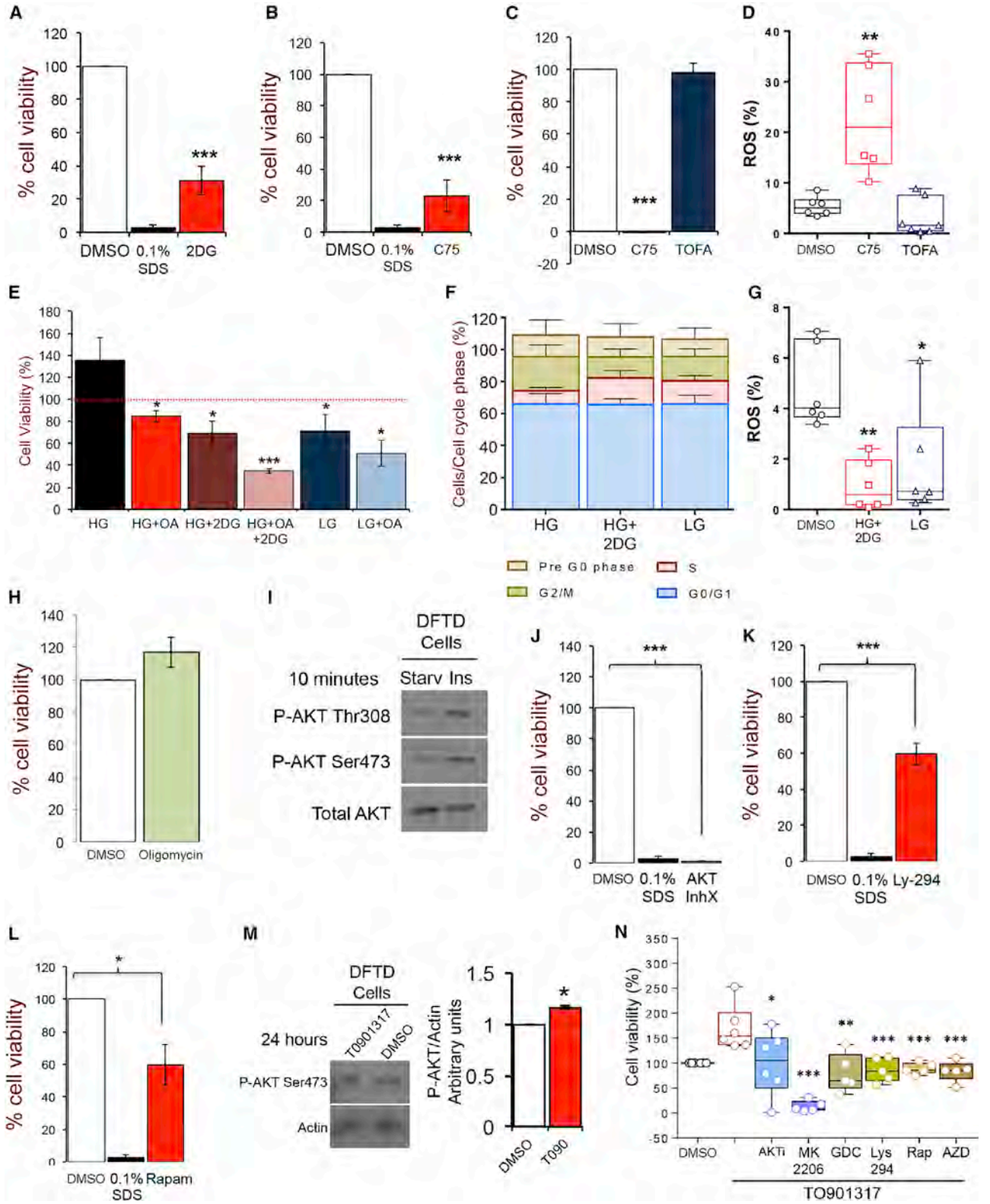

Figure 2. Glucose metabolism drives the proliferation of DFTD4 cells

(A–C) DFTD4 cell proliferation in response to (A) 2-DG (1 mM), (B) C75 (1 μM), and (C) TOFA (3 μM) in comparison to vehicle (DMSO)-treated cells. 0.1% SDS was used as the positive control, causing 100% toxicity. Six independent experiments were performed in duplicate.

(legend continued on next page)

(25-OHC), and 27S-hydroxycholesterol (27-OHC), collectively termed oxysterols (Calkin and Tontonoz, 2012; Mutemberezi et al., 2016; Russell, 2000). 24-OHC, similar to T0901317, reduced the cholesterol content in DFTD4 cells (Figure S1G) and was the only oxysterol capable of exacerbating DFTD4 cell proliferation in a dose-dependent manner (1 and 10 μM), whereas 25-OHC and 27-OHC either had no effect (27-OHC, 1 μM, Figure 1H) or decreased cell proliferation (25-OHC, 1 μM, Figure 1H; 27-OHC and 25-OHC, 10 μM, Figure 1I). When we examined the other DFTD cells, 24-OHC, like in DFTD4 cells, was the predominant oxysterol stimulating cell proliferation with a significant increase in DFTD2 cell population (Figures S1H and S1I). However, 24-OHC-treated DFTD1 only exhibited a trend to increase cell growth (Figure S1H; $p = 0.0768$). Moreover, 27-OHC and 25-OHC did not show a significant effect in DFTD1. However, in DFTD2 cells, only 27-OHC promoted cell growth, albeit less than that seen using 24-OHC, whereas 25-OHC exhibited no effect (Figure S1I). Therefore, our experiments unravel a partial cell-type-dependent heterogeneity in the LXR-oxysterol response in DFTD cells (Figures 1H and 1I; Figures S1H and S1I). Activation of LXR signaling leads to the stimulation of glycolysis with an impact on the metabolic pathways producing ATP. To elucidate the metabolic mechanism underlying T0901317-induced proliferation in DFTD cells, we examined the glycolytic flux and mitochondrial respiration using Seahorse technology. We observed no modifications in glycolysis in response to either T0901317 or 24-OHC (Figures S1J and S1K) in FIBs. In contrast, in DFTD cells, the activation of LXR signaling by T0901317 and 24-OHC links the stimulation of cell proliferation to a metabolic switch represented by a reduction of oxidative phosphorylation and mitochondrial respiration (Figures 1J and 1K) and an elevation of aerobic glycolysis, also known as the Warburg effect (Figures 1L and 1M).

DFTD cell proliferation relies on aerobic glycolysis

Because LXR nuclear receptors are also stimulating glycolysis and *de novo* lipogenesis, we investigated the impact of inhibiting these two metabolic pathways on the proliferation and viability of DFTD4 cells. Both 2-deoxy-glucose (2-DG), an allosteric inhibitor of glycolysis, and cerulenin (C75), which inhibits FASN activity, prevented DFTD4 proliferation (Figures 2A–2C; Figures S2A–S2D) in association with an increase of reactive oxygen species (ROS) (Figure 2D). However, TOFA, another inhibitor of lipogenesis targeting acetyl-coenzyme A (CoA) carboxylase (ACC), did not exhibit cytotoxic effects (Figure 2C; Figures S2C and S2D) or stimulate the generation of ROS (Figure 2D; Table S2). This agrees with the null effects observed in 5-aminoimidazole-4-carboxamide ribonucleotide (AICAR)-treated DFTD4 cells (Figure 1A), a compound that phosphorylates and inactivates ACC, suggesting that DFTD4 proliferation does not rely on stimulation of *de novo* lipogenesis. Instead, and in support of dependence on glycolysis, DFTD4 cells exhibited higher ratios of proliferation in high glucose (HG, 25 mM glucose) conditions but significant lower proliferation in low glucose (LG, 5 mM glucose) conditions, which mimicked the effect of 2-DG (Figure 2E). Supplementation of 2-DG with oleic acid (OA) or LG with various fatty acids, including OA, a mix of linoleic and oleic acid (LOA), or palmitic acid (PA) as an alternative source of energy, did not restore the growth ratios in 2-DG- or LG-treated DFTD4 cells (Figure 2E; Figure S2E). This suggested that fatty acids do not substitute for carbohydrates as a source of energy and cellular scaffolds to sustain the proliferation of DFTD cells. Both 2-DG and LG (24 h) treatment caused a trend of cell-cycle arrest in the S phase of mitosis (Figure 2F; Table S3), with an alteration in the cellular levels of ROS (Figure 2G; Table S2). Inhibition of the generation of mitochondrial ATP by targeting ATP synthase by oligomycin did not suppress proliferation (Figure 2H; Figures S2F and S2G), suggesting again that DFTD cells exhibit a preference for glycolytic metabolism to proliferate. To support this hypothesis, first we questioned whether DFTD4 cellular glucose metabolism is regulated by mechanisms similar to those in mammalian cells. For this, we examined the activation of the AKT pathway in response to insulin, a major regulatory mechanism for glucose transport and metabolism. Analysis of AKT phosphorylation by immunoblot revealed that phosphorylation in both serine-473 (Ser473) and threonine-308 (Thr308) residues and sensitivity to insulin are evolutionary conserved in DFTD cells (Figure 2I). Then, we questioned whether proliferation of DFTD depends on the activation of AKT signaling, including its effector phosphatidylinositol 3-kinase (PI3K) and its target mTOR. Answering this, the AKT inhibitors IX (InhX), MK2206, or GDC-0068; the PI3K inhibitor Lys294002; and the mTOR inhibitors rapamycin and AZD8055 prevented the proliferation of DFTD cells (Figures 2J–2L; Figures S3A–S3J). Our analysis of the Tasmanian devil genome revealed the existence of only *AKT1* and *AKT3* genes, not *AKT2*. We also deciphered that the devil genome contains both LXR isoform genes, *LXRα* and *LXRβ*, although gene expression analysis showed that DFTD cells do not express

(D) ROS generation by C75 and TOFA in response to vehicle (DMSO). Seven independent experiments were performed.
(E) DFTD4 cell proliferation in response to high glucose (HG, 25 mM) and low glucose (LG, 5 mM) for 48 h alone or in combination with oleic acid (OA, 200 μM) and 2-DG (1 mM) in comparison to medium glucose (11 mM; red line). Five independent experiments were performed in duplicate.
(F) Percentage of cells in the difference cell-cycle phases in response to HG, HG+2-DG, and LG. Six independent experiments were performed.
(G) ROS generation by HG, HG+2-DG, and LG. Six independent experiments were performed.
(H) DFTD4 cell proliferation in response to oligomycin (5 μg/mL, n = 4).
(I) Representative immunoblot of three independent experiments showing conserved phosphorylation of AKT in the Thr308 and Ser473 residues in response to insulin (5 U/mL) activation for 10 min in comparison to starved (Starv) DFTD4 cells not treated with insulin.
(J–L) DFTD4 cell proliferation for 48 h in response to (J) AKT inhibitor X (AKTi, 1 μM), (K) PI3K inhibitor LY294002 (Lys294, 30 μM), and (L) mTOR inhibitor rapamycin (1 nM). Five independent experiments (except for AKTi, which is the result of three experiments) were performed in duplicate.
(M) Representative immunoblot and band intensity quantification related to actin of three independent experiments showing upregulated AKT phosphorylation in the Ser473 residue in response to T090 (2.5 μM, 24 h) in comparison to vehicle (DMSO) in DFTD4 cells.
(N) DFTD4 cell proliferation in response to T0901317 alone or in combination with AKTi (1 μM), MK2206 (10 μM), and GDC-0065 (GDC, 1 μM), PI3K inhibitor Lys294 (30 μM), mTOR inhibitor rapamycin (1 nM), and mTORC1 and mTORC2 inhibitor AZD8055 (1 μM).
Data are shown as mean ± SEM. *$p < 0.05$, **$p < 0.01$, ***$p < 0.001$, ****$p < 0.0001$. The proliferation experiments were performed at 48 h. All other described experiments were performed at 24 h.

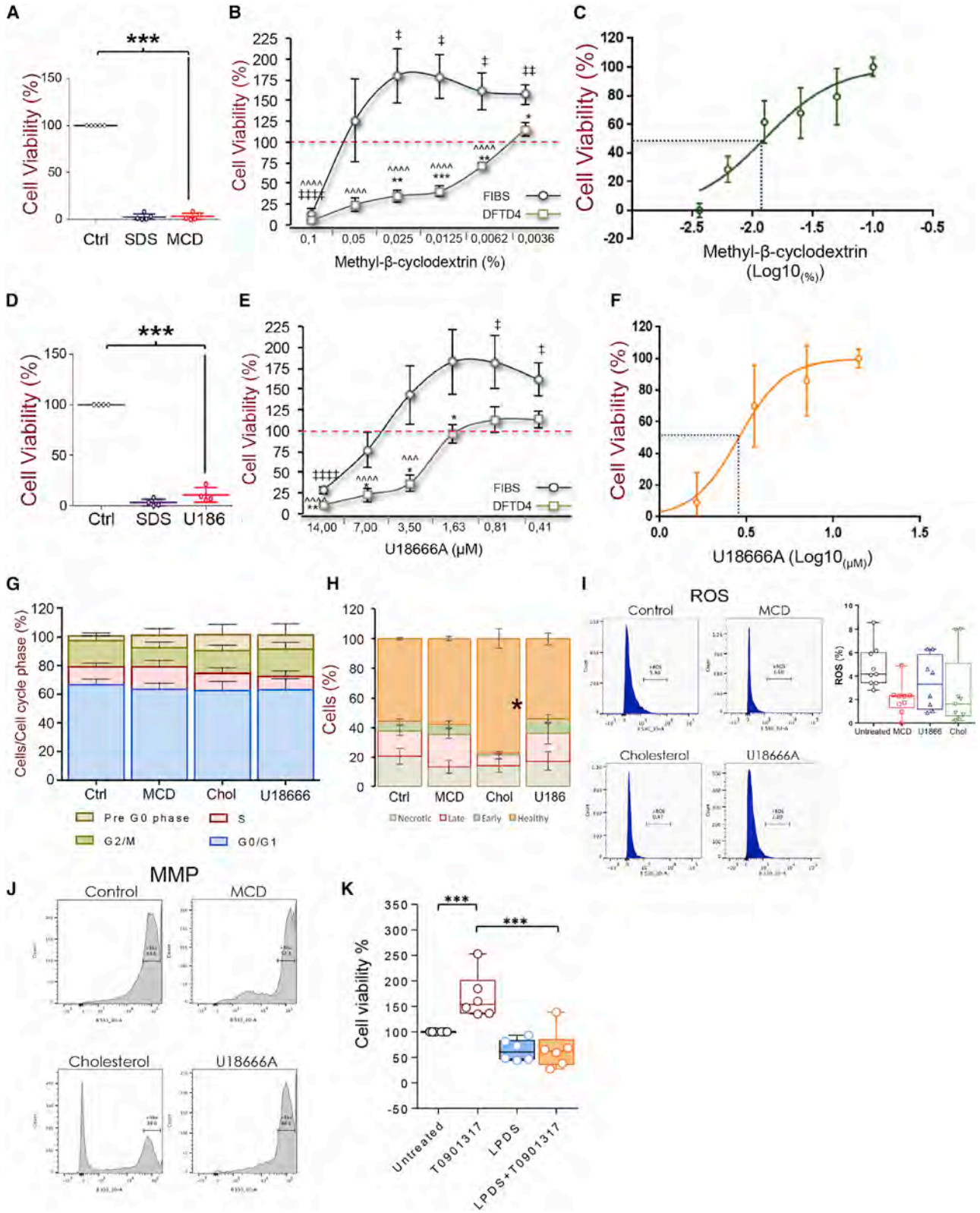

(legend on next page)

LXRα and only express LXRβ (data not shown). First, 24-h treatment with T0901317 did not stimulate the expression of LXRβ, AKT1, or AKT3 (Figure S3K). However, T0901317 increased the phosphorylation of AKT at the Ser473 residue (Figure 2M). Next, we assessed whether T0901317 stimulation of DFTD growth depends on AKT signaling. Chemical repression of PI3K, AKT, and mTORC1 and mTORC2 activities using the diverse inhibitors described earlier abrogated T0901317-induced stimulation of the proliferation of DFTD4 cells (Figure 2N). Hence, we postulate that DFTD cells, like human tumor cells, rely on aerobic glycolysis rather than oxidative phosphorylation to proliferate in a LXRβ- and AKT-dependent manner.

Cholesterol homeostasis sustains DFTD proliferation

Cells have developed complex mechanisms, including LXR and 24-OHC signaling cascades, to tightly regulate the content, distribution, and metabolism of sterols by balancing intracellular synthesis, dietary cellular uptake, intracellular trafficking, and removal of cholesterol excess (Parton and del Pozo, 2013; Pommier et al., 2010; Rothblat et al., 1999; Simons and Ikonen, 2000; Sorrentino et al., 2014). Conversely, cholesterol constitutes a molecular core in which the function of receptors and signaling proteins, enzymes, protein sorting, and lipid metabolism-related signaling cascades (i.e., SREBPs and FXRα/LXR) converge to regulate cell proliferation and apoptosis (Parton and del Pozo, 2013; Pommier et al., 2010; Silvente-Poirot and Poirot, 2012; Simons and Ikonen, 2000; Simons and Sampaio, 2011). Upon imbalance, the signaling cascades underlying cell growth and death might have key tissue-specific and systemic consequences that can lead either to tumor growth and metastasis or to regression of cancer (Calkin and Tontonoz, 2012; Mutemberezi et al., 2016; Rothblat et al., 1999; Silvente-Poirot and Poirot, 2012; Simons and Ikonen, 2000). Therefore, with the observed implications of LXR signaling and cholesterol overloading in DFTD cells, we suggest that targeting cholesterol homeostasis may constitute a feasible therapeutic strategy against DFTD.

To test this hypothesis, we assessed how sequestration of membrane cholesterol by β-methyl-cyclodextrin (MCD) affects the viability and proliferation of DFTD cells. MCD is a water-soluble, membrane-impermeable molecule that binds free cholesterol with high affinity without affecting the cellular cholesterol content (Rothblat et al., 1999). Incubation of DFTD4 cells in medium containing 0.05% MCD for 48 h caused a significant reduction in the number of cells (Figure 3A), results that were recapitulated in DFTD1 and DFTD2 cells (Figures S1E and S1F). Thus, a dose-response experiment performed in untreated and MCD-treated DFTD4 cells versus FIBs demonstrated that MCD impairs the proliferation of DFTD4 cells in a cell-autonomous-specific manner (Figure 3B). MCD at 0.1%, 0.05%, 0.025%, and 0.0125% significantly reduced the number of DFTD4 cells after 48 h, with an EC_{50} of 0.0099% (Figure 3C). Conversely, with the exception of 0.1%, at which MCD was cytotoxic, concentrations $\leq$0.05 were not harmful but instead promoted the proliferation of FIBs (Figure 3B). Both plasma and endomembrane networks depend on cholesterol trafficking among organelles. Hence, to test whether the intracellular cholesterol flux compromises the viability of DFTD cells, we used U18666A, a major inhibitor of the intracellular trafficking of cholesterol (Cenedella, 2009) (Figure 3D; Figures S1E and S1F). As seen in both MCD-treated and exogenous cholesterol-treated DFTD cells, U18666A induced suppression of cholesterol dynamics and compromised the proliferation of the cells, even at a low concentration (i.e., 3.50 μM). Conversely at the EC_{50} of U18666A in DFTD4 cells (2.85 μM, Figures 3E and 3F), U18666A treatment of FIBs resulted in a trend to increase their proliferation ratio, which was maintained over decreasing concentrations (i.e., 1.63, 0.81, and 0.41 μM) (Figure 3E). Thus, these results suggest that in a cell-type-dependent manner, cellular cholesterol balance determines the proliferative capacity of tumorigenic and non-tumorigenic Tasmanian devil cells by several mechanisms, which may include those regulating the crosstalk between the intracellular compartments during the transduction of signaling cascades and the cellular content of total and free cholesterol.

Mechanistically, at 24 h of cholesterol sequestration with MCD, supplementation with exogenous cholesterol, and U18666A-induced inhibition of the intracellular trafficking of cholesterol, did not affect cell-cycle progression in DFTD4 cells (Figure 3G; Table S3). Accordingly, MCD-, cholesterol-, and U18666A-cholesterol interventions did not induce cell apoptosis or necrosis in DFTD4 cells (Figure 3H; Table S4). Instead, the

Figure 3. Manipulation of cholesterol homeostasis compromises DFTD cell proliferation

(A) Effect of MCD (0.05%) on DFTD4 cell proliferation by MTT assay. DMSO was used as the vehicle control, and 0.1% SDS was used as the positive control, causing 100% toxicity. Five independent experiments were performed in duplicate.

(B) Dose-dependent effect of MCD on cell proliferation of DFTD4 cells in comparison to FIBs. Six independent experiments were performed in duplicate.

(C) Cell viability of DFTD4 cells treated with a range of MCD concentrations showing the EC_{50} (log 10 scale).

(D) Effect of U18666A (7 μM) on DFTD4 cell proliferation. Four independent experiments were performed in duplicate.

(E) Dose-dependent effect of U18666A on cell proliferation of DFTD4 cells in comparison to FIBs. Six independent experiments were performed in duplicate.

(F) Cell viability of DFTD4 cells treated with a range of U18666A concentrations showing the EC_{50} (log 10 scale).

(G) Cell-cycle phase analysis (G0/G1, S, and G2/M phases) in DFTD4 cells exposed to MCD (0.05%), cholesterol (120 μg/mL), or U18666A (7 μM). Six independent experiments were performed.

(H) Percentage of DFTD4 apoptotic cells exposed to MCD, cholesterol, and U18666A was assessed using an annexin V-fluorescein isothiocyanate (FITC) assay. Three independent experiments were performed.

(I) Representative ROS measurement in DFTD4 cells exposed to MCD (0.05%), cholesterol (120 μg/mL), and U18666A (7 μM) and their quantification. Eight independent experiments were performed.

(J) Representative experiment of mitochondrial membrane potential (MMP) in DFTD4 cells exposed to MCD (0.05%), cholesterol (120 μg/mL), and U18666A (7 μM), as well as their overall quantification. Five independent experiments were performed.

(K) DFTD4 cell proliferation in 10% fetal bovine serum (FBS) or in 10% delipidated (lipoprotein-deficient serum [LPDS]) serum-supplemented culture media without the presence of the T0901317 (2.5 μM) LXR agonist. DMSO is used as a vehicle control. Four independent experiments were performed in duplicate. Data are shown as mean ± SEM. *$p < 0.05$, **$p < 0.01$, ***$p < 0.001$.

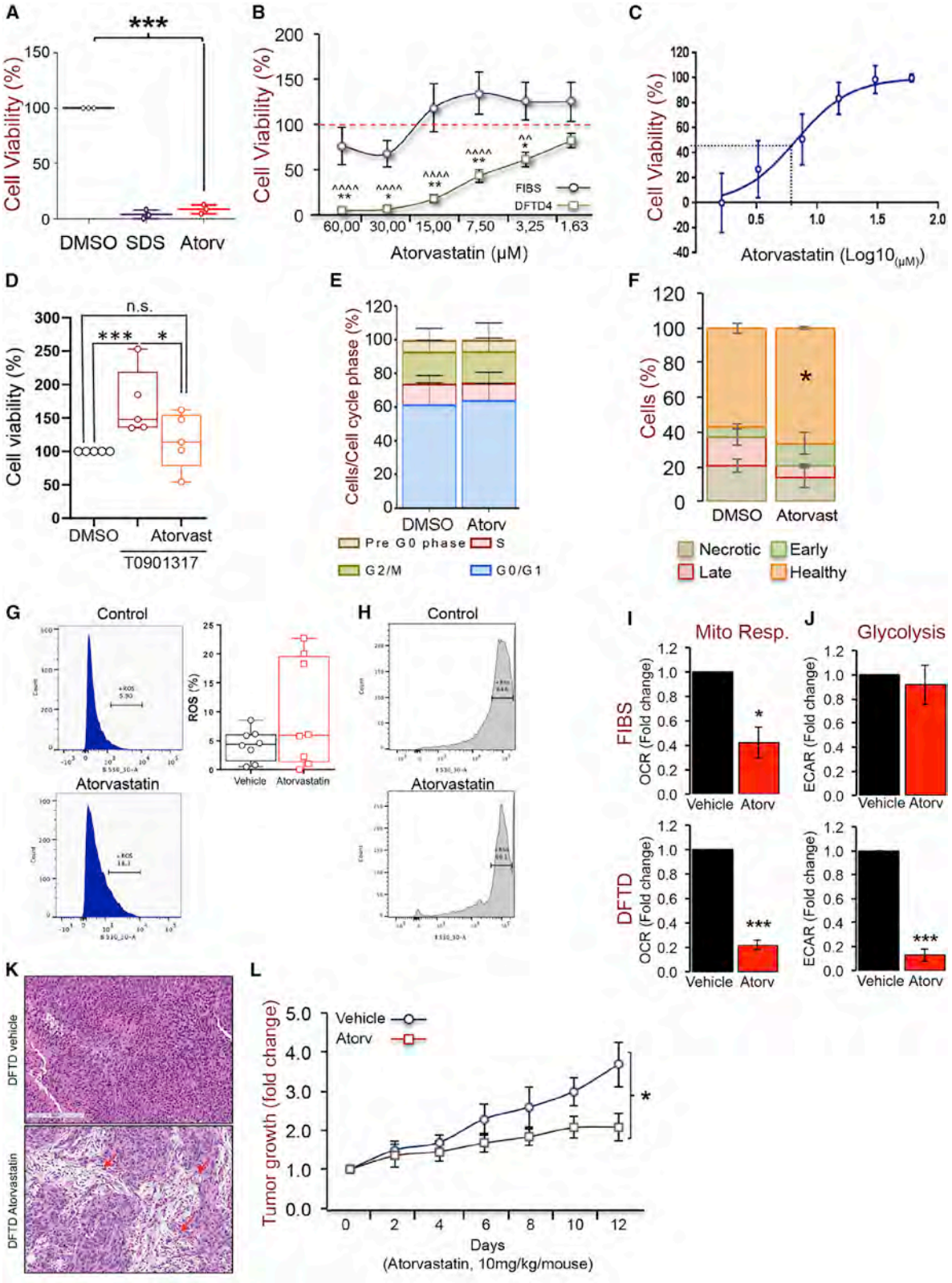

(legend on next page)

number of healthy cells under MCD and U18666A conditions was similar to the number observed in the untreated DFTD cell population, whereas cholesterol-treated DFTD cells exhibited a remarkable increase in the proportion of healthy cells (Figure 3H; Table S4). Altogether, these data support our proposal that disruption of cholesterol homeostasis compromises the long-term viability of DFTD cells. Elevated generation of ROS and reduction of the mitochondrial membrane potential (MMP) are both hallmark parameters during cellular stress and under cytotoxic stimuli. Rather than augmenting, from all approaches we assessed to disrupt cholesterol homeostasis (MCD, cholesterol, and U18666A), only MCD significantly decreased ROS cellular content (Figure 3I; Table S2), whereas the impact on MMP was minimum among treatments (Figure 3J; Table S5). This suggests that cholesterol might regulate the proliferation of DFTD cells via specific molecular mechanisms. Indeed, T0901317-treated DFTD4 cells exhibited elevated expression of the HMG-CoA reductase (HMGCR) gene (Figure 1C), coding the major enzyme for the synthesis of cholesterol, suggesting that when the cholesterol levels are below a specific threshold, DFTD cells may try to activate compensatory mechanisms to maintain a minimum cholesterol content threshold. Accordingly, culture of DFTD cells in medium supplemented with delipidated serum (without lipoproteins and therefore cholesterol) impairs cell growth and prevented T0901317-induced proliferation of DFTD4 cells (Figure 3K).

Pharmacological targeting of cholesterol synthesis by atorvastatin inhibits DFTD-xenograft tumors' growth

Reduced intensity of filipin staining in DFTD cells suggested that MCD treatment reduce the cellular cholesterol, in accordance with cholesterol overloading (Figure S4A). DFTD cells cultured in cholesterol-enriched culture media exhibited a stronger intensity of filipin staining, and U18666A treatment altered the distribution of cellular cholesterol in comparison to DFTD cells in standard culture conditions (Figure S4A). Based on the dramatic impact of the modulation of the cellular cholesterol on the viability and growth of DFTD cells, we assessed the effect of statins, the preferred drugs used to inhibit cholesterol synthesis to reduce blood cholesterol levels in the treatment of cardiovascular disorders and that have also been proven to exhibit anti-tumorigenic properties, and the clinical impact on patients (Cenedella, 2009; Pelton et al., 2014; Rao et al., 1998; Zhang et al., 2014). Hence, we hypothesized that statins might also have anti-proliferative (and thus anti-tumoral) activity in DFTD cells. Accordingly, atorvastatin reduced cholesterol content (Figure S4B) and drastically reduced the number of DFTD cells *in vitro* (Figure 4A; Figures S4C and S4D), exhibiting minimal overall effects on FIBs (Figure 4B) with an EC_{50} of 6.66 μM in DFTD4 (Figure 4C). Atorvastatin also prevented the cell proliferation induced by the LXR agonist T0901317 (Figure 4D), supporting the preceding hypothesis that DFTD cells might require minimum cellular cholesterol content to grow. At the cellular level, 24-h treatment with atorvastatin did not affect the cell cycle of DFTD cells (Figure 4E; Table S3). In addition, although there was a trend to increase DFTD cells entering early apoptosis, the number of atorvastatin-treated DFTD4 healthy cells was significantly elevated after 24 h (Figure 4F; Table S4), resembling the effects of MCD, exogenous cholesterol, and U18666A. Furthermore, atorvastatin did not affect either ROS (Figure 4G; Table S2) or MMP (Figure 4H; Table S5) in DFTD4 cells. Metabolic assessment of DFTD cells using Seahorse technology showed that 24-h atorvastatin treatment caused a blackout of the energy system in DFTD cells in comparison to FIBs (Figures 4I and 4J). Although atorvastatin reduced mitochondrial respiration in FIBs, this was significantly more pronounced and almost completely ablated in DFTD4 cells. In addition, in a cell-type-dependent manner, atorvastatin inhibited glycolysis in DFTD4 cells but had no effect on FIBs (Figures 4I and 4J). Because atorvastatin compromises the viability of DFTD cells *in vitro*, we postulated that it may be beneficial in the treatment of DFTD tumor growth *in vivo*. To test this, and as a proof-of-concept experiment, we examined the anti-tumorigenic activity of atorvastatin in comparison to vehicle in DFTD-xenograft tumors induced in nude mice. As reported previously (Montero et al., 2008), atorvastatin (10 mg/kg/mouse every 2 days for 12 days) did not result in deleterious effects on mouse health (data not shown). However, histology examination by hematoxylin and eosin (H&E) staining showed that atorvastatin treatment increased necrosis in DFTD-xenograft

Figure 4. Atorvastatin inhibits DFTD cell proliferation and DFTD-xenograft tumor growth

(A) Effect of atorvastatin (Atorv, 15 μM) on DFTD4 cell proliferation after 48 h of exposure by MTT assay. DMSO was used as the vehicle control, and 0.1% SDS was used as the positive control, causing 100% toxicity. Three independent experiments were performed in triplicate.

(B) Dose-dependent effect of Atorv on cell proliferation in DFTD4 and compared with FIBs.

(C) Cell viability of DFTD4 cells treated with a range of Atorv concentrations showing the EC_{50} (log 10 scale). Six independent experiments were performed in duplicate.

(D) DFTD4 cell proliferation in the presence of the T0901317 (2.5 μM) LXR agonist alone or in combination with Atorv in comparison to untreated cells. Six independent experiments were performed in duplicate.

(E) Cell-cycle phase analysis in DFTD4 cells exposed to Atorv (15 μM) or DMSO for 24 h. Five independent experiments were conducted.

(F) Percentage of DFTD4 apoptotic cells exposed to Atorv (15 μM) for 24 h. Three independent experiments were performed.

(G) Representative ROS measurement in DFTD4 cells exposed to Atorv (15 μM) for 24 h. Eight independent experiments were performed.

(H) Representative experiment of MMP in DFTD4 cells exposed to Atorv (15 μM) for 24 h. Six independent experiments were performed.

(I) Mitochondrial respiration (OCR) in Atorv-treated FIBs and DFTD4 cells in comparison to vehicle (DMSO), represented as fold change of picomoles per minute.

(J) Glycolytic flux (ECAR) in Atorv-treated FIBs and DFTD4 cells in comparison to vehicle (DMSO), represented as fold change of milli-pH per minute.

(K) Hematoxylin and eosin staining in 12-day DFTD-xenograft tumors exposed to vehicle or Atorv (10 mg/kg/mouse). Red arrows indicate areas of visible fibrosis within the DFTD-xenograft tumors. Scale bar represents 300 μm.

(L) DFTD-xenograft tumor growth (fold change relative to day 0) exposed to vehicle or Atorv (10 mg/kg/mouse). The progression of ten tumors per group was examined over 12 days.

For OCR and ECAR, four independent experiments were performed in five replicates. Data are shown as mean ± SEM. Statistical analyses are relative to untreated cells and are represented as *$p < 0.05$, **$p < 0.01$, ***$p < 0.001$, and ****$p < 0.0001$.

tumors (Figure 4K). Moreover, atorvastatin, significantly reduced the growth of DFTD-xenograft tumors *in vivo* (Figure 4L), underscoring its therapeutic potential as a treatment against DFTD in Tasmanian devils.

DISCUSSION

The critical expansion of DFTD threatening the conservation of the Tasmanian devil has been facilitated by limited comprehensive analysis of the molecular mechanisms driving the proliferation of DFTD cells. Only recently has it been shown that tyrosine kinases, DNA repair inhibitors, and ERBB or STAT3 inhibitors could have therapeutic potential against DFTD (Kosack et al., 2019; Stammnitz et al., 2018). Here, we have identified that in a cell-autonomous manner, cholesterol homeostasis exerts an essential role in regulating the proliferation of DFTD cells. Using both cellular and molecular biological approaches, we conclude that for efficient proliferation, DFTD cells maintain tight control of the mechanisms regulating cellular cholesterol at different levels (i.e., compartmentalization, synthesis, and uptake). Moreover, via Seahorse metabolic analysis in DFTD cells, together with pharmacological manipulation of PI3K/AKT/mTOR signaling, we provide compelling evidence that the oncogenic impact of the activation of LXR signaling may occur through the nuclear receptor LXRβ in a cell-type- and oxysterol-type-specific manner that promotes carbohydrate metabolism in a AKT-dependent manner. We attempted to provide more supportive insight into this conclusion via genetic manipulation of DFTD cells using CRISPR-Cas9 technology (data not shown). Indeed, we were able to generate AKT1 and LXRβ-deficient DFTD4 cells. However, DFTD cells happen to exhibit significant cytotoxic sensitivity toward the transfer of genetic material and genetic manipulation. Transfection strategies (lipofectamine and other similar reagents) of vectors overexpressing GFP- or hemagglutinin (HA)-tagged AKT isoforms resulted in cellular death (data not shown). Similar results occurred when we attempted to transfect vectors expressing Cas9 protein complexed with single guide RNAs (sgRNAs) targeting AKT1, AKT3, or LXRβ. We were partially successful using electroporation and generated DFTD cell pooled populations lacking AKT1 (83%) or LXRβ (55%) wild-type sequence in comparison to control DFTD cells transfected with sgRNAs against the ROSA (*ROSA26*) locus, which only exists in mice, so it is commonly used as a non-targeting control. However, electroporation caused loss of proliferative capacity and sensitivity to T0901317 over several cell passages. We also observed this phenotype in electroporated DFTD cells without sgRNA. We emphasize that generation of DFTD cells deficient in key genes for their proliferation is crucial to full comprehension of the mechanisms driving the development of DFTD in Tasmanian devils. Our results warrant investigation to optimize protocols that apply CRISPR-Cas9 technologies in DFTD cells. Nevertheless, we believe that the results presented in this study constitute a significant step forward in our molecular understanding of the nature of the proliferation of DFTD cells, mainly when activation of LXR signaling via agonists and 24-OHC has been proven to exhibit tumor suppressor properties in human cancer cells, particularly from the brain (i.e., glioblastoma). Thus, this study suggests that cholesterol, LXRβ, and the cellular machinery for DFTD cell growth constitute an intricate molecular network that differs from the canonical signaling axis observed in human cancer cells (Bensinger et al., 2008; Bovenga et al., 2015; Villa et al., 2016) and that requires low cholesterol content to stimulate DFTD growth. However, reduced DFTD cell growth in response to sequestration of free cholesterol and inhibition of the biosynthesis, as well as intracellular trafficking of cholesterol, suggests that to proliferate, DFTD cells require a minimum cellular cholesterol content threshold and communication among the intracellular pools of cholesterol.

Cell-type-dependent sensitivity to oxysterol reveals that DFTD cells exhibit oxysterol-LXR signaling heterogeneity. 24-OHC is a prominent pro-oncogenic LXR-ligand, the activities of which in DFTD cells may be explained by the common neuronal cellular origin shared between 24-OHC and DFTD cells. Although DFTD cells originated from Schwann cells, 24-OHC is known as a brain-derived oxysterol or cerebrosterol because of the high expression levels of cholesterol 24-hydroxylase (CYP46A1), the enzyme responsible for 24-OHC synthesis, in neurons (Lo Sasso et al., 2010). Moreover, because 25-OHC and 27-OHC exhibited null pro-oncogenic or repressive activities on cell proliferation, we postulate that LXRβ signaling might exert a dual role in the progression of DFTD.

Although these data provide a mechanistic model to better understand DFTD progression, experiments in DFTD-xenograft tumors *in vivo* demonstrate that statins may constitute a potential therapeutic approach to treat DFTD disease and therefore contribute to the conservation of the Tasmanian devil species. This is in agreement with studies in cultured human tumor cells, human cancer mouse models, and clinical trials, which together have recommended that statins may work as anticancer drugs or as adjuvants in combination with standard antitumoral therapies (Jiang et al., 2014; Nielsen et al., 2012; Tsan et al., 2012) and hence validate the feasibility of applying our approach in further *in vivo* studies in Tasmanian devils. Moreover, the data obtained *in vitro* suggest that targeting carbohydrate metabolism and even *de novo* lipogenesis via treatment with C75 may constitute feasible approaches against DFTD. 2-DG and the AKT inhibitors MK2206 and GDC-0068 are being used in clinical trials against solid tumors (Prêtre and Wicki, 2018; Raez et al., 2013), whereas the mTOR inhibitor rapamycin and the FDA-approved rapamycin analogs (rapalogs) have already been proposed as therapeutic regimes against various solid and soft tumors (Li et al., 2014). C75 is more controversial, because its anti-tumorigenic effects emerge from the accumulation of malonyl-CoA rather from the inhibition of lipogenesis (Thupari et al., 2001), which is in agreement with our data showing opposite results from C75- and TOFA-treated DFTD cells. Therefore, warranting further *in vivo* investigations, we postulate that biochemical approaches to manipulate cholesterol-dependent DFTD cell proliferation via statins alone or in combination with 2-DG, AKT inhibitors, rapamycin/rapalogs, or C75 may prevent, or at least reduce, the progression of DFTD, which may greatly assist in ongoing management plans for the conservation of the Tasmanian devil species. In summary, although implementation of these strategies in wild Tasmanian devils may constitute a significant challenge, we believe that validation of the therapeutic potential of statins (atorvastatin) and drugs targeting carbohydrate

metabolism in diseased animals in captivity would be a beneficial alternative approach, in conjunction with current management strategies.

STAR★METHODS

Detailed methods are provided in the online version of this paper and include the following:

- KEY RESOURCES TABLE
- RESOURCE AVAILABILITY
  - Lead contact
  - Materials availability
  - Data and code availability
- EXPERIMENTAL MODEL AND SUBJECT DETAILS
  - Animal studies
- METHOD DETAILS
  - DFTD cell lines and cell culture
  - Cell viability
  - Seahorse glycolysis and mitochondrial respiration flux analysis
  - Filipin staining
  - Knockout of LXRβ, AKT1 and AKT3 in DFTD4 cells
  - Western blots
  - Cell cycle
  - Cell apoptosis
  - Reactive oxygen species
  - Mitochondria membrane potential
  - Real time PCR
  - Measurement of the cholesterol content
- QUANTIFICATION AND STATISTICAL ANALYSIS

SUPPLEMENTAL INFORMATION

Supplemental Information can be found online at https://doi.org/10.1016/j.celrep.2021.108851.

ACKNOWLEDGMENTS

DFTD and FIB cell lines were obtained from the Department of Primary Industries, Parks, Water and Environment (DPIPWE) in Tasmania. The cell lines were established as part of a management plan and adhered to a standard operating practice. We thank Prof. Rajiv Khanna for allowing us to access his fluorescence-activated cell sorting (FACS) facilities at QIMR Berghofer MRI. We thank also Associate Professor Marco Herold from the Walter and Eliza Hall Institute of Medical Research for assisting and providing the facilities of his laboratory to attempt to develop CRISPR-Cas9 AKT1, AKT3, and LXRβ knockout DFTD cells. M.P.I. has been supported by the AMAROUT Marie Curie program (291803-AMAROUT II) and the TALENTO Program of the Regional Madrid Government (2018-T1/BIO-11262); G.A.R. is supported by the National Health and Medical Research Council of Australia (NHMRC) (APP1064533) and the NHMRC Senior Research Fellowship (APP1061332); and M.A.F.-R. is supported by the TALENTO Program of the Regional Madrid Government (2016/T1-BIO-1854).

AUTHOR CONTRIBUTIONS

M.P.I. and M.A.F.-R. conceived, designed, and performed most experiments, interpreted the data, and wrote the manuscript. Y.L.-M. performed gene expression analysis and metabolic assays with Seahorse equipment. M.G.N. carried out gene expression with real-time PCR. M.M.-U. measured the cholesterol content in devil cells. L.G. and M.P. designed and carried out the development of CRISPR-Cas9-LXRβ and AKT-deficient cells. L.F.C.-M. and P.J.F.-M. assisted in the performance and analysis of the seahorse metabolic experiments. G.A.R. provided reagents and intellectual input. All authors read and provided feedback on the manuscript.

DECLARATION OF INTERESTS

The authors declare no competing interests.

INCLUSION AND DIVERSITY

One or more of the authors of this paper self-identifies as an underrepresented ethnic minority in science.

Received: May 1, 2019
Revised: November 2, 2020
Accepted: February 17, 2021
Published: March 16, 2021

REFERENCES

Bensinger, S.J., Bradley, M.N., Joseph, S.B., Zelcer, N., Janssen, E.M., Hausner, M.A., Shih, R., Parks, J.S., Edwards, P.A., Jamieson, B.D., and Tontonoz, P. (2008). LXR signaling couples sterol metabolism to proliferation in the acquired immune response. Cell *134*, 97–111.

Bovenga, F., Sabbà, C., and Moschetta, A. (2015). Uncoupling nuclear receptor LXR and cholesterol metabolism in cancer. Cell Metab. *21*, 517–526.

Brown, G.K., Tovar, C., Cooray, A.A., Kreiss, A., Darby, J., Murphy, J.M., Corcoran, L.M., Bettiol, S.S., Lyons, A.B., and Woods, G.M. (2016). Mitogen-activated Tasmanian devil blood mononuclear cells kill devil facial tumour disease cells. Immunol. Cell Biol. *94*, 673–679.

Calkin, A.C., and Tontonoz, P. (2012). Transcriptional integration of metabolism by the nuclear sterol-activated receptors LXR and FXR. Nat. Rev. Mol. Cell Biol. *13*, 213–224.

Cenedella, R.J. (2009). Cholesterol synthesis inhibitor U18666A and the role of sterol metabolism and trafficking in numerous pathophysiological processes. Lipids *44*, 477–487.

Duval, C., Touche, V., Tailleux, A., Fruchart, J.C., Fievet, C., Clavey, V., Staels, B., and Lestavel, S. (2006). Niemann-Pick C1 like 1 gene expression is down-regulated by LXR activators in the intestine. Biochem. Biophys. Res. Commun. *340*, 1259–1263.

Fernandez-Rojo, M.A., Deplazes, E., Pineda, S.S., Brust, A., Marth, T., Wilhelm, P., Martel, N., Ramm, G.A., Mancera, R.L., Alewood, P.F., et al. (2018). Gomesin peptides prevent proliferation and lead to the cell death of devil facial tumour disease cells. Cell Death Discov. *4*, 19.

Flies, A.S., Lyons, A.B., Corcoran, L.M., Papenfuss, A.T., Murphy, J.M., Knowles, G.W., Woods, G.M., and Hayball, J.D. (2016). PD-L1 is not constitutively expressed on Tasmanian Devil Facial Tumor Cells but is strongly upregulated in response to IFN-γ and can be expressed in the tumor microenvironment. Front. Immunol. *7*, 581.

Ikonomopoulou, M.P., Fernandez-Rojo, M.A., Pineda, S.S., Cabezas-Sainz, P., Winnen, B., Morales, R.A.V., Brust, A., Sánchez, L., Alewood, P.F., Ramm, G.A., et al. (2018). Gomesin inhibits melanoma growth by manipulating key signaling cascades that control cell death and proliferation. Sci. Rep. *8*, 11519.

Jiang, P., Mukthavaram, R., Chao, Y., Nomura, N., Bharati, I.S., Fogal, V., Pastorino, S., Teng, D., Cong, X., Pingle, S.C., et al. (2014). *In vitro* and *in vivo* anticancer effects of mevalonate pathway modulation on human cancer cells. Br. J. Cancer *111*, 1562–1571.

Kosack, L., Wingelhofer, B., Popa, A., Orlova, A., Agerer, B., Vilagos, B., Majek, P., Parapatics, K., Lercher, A., Ringler, A., et al. (2019). The ERBB-STAT3 Axis Drives Tasmanian Devil Facial Tumor Disease. Cancer Cell *35*, 125–139.e9.

Li, J., Kim, S.G., and Blenis, J. (2014). Rapamycin: one drug, many effects. Cell Metab. *19*, 373–379.

Lo Sasso, G., Celli, N., Caboni, M., Murzilli, S., Salvatore, L., Morgano, A., Vacca, M., Pagliani, T., Parini, P., and Moschetta, A. (2010). Down-regulation of the LXR transcriptome provides the requisite cholesterol levels to proliferating hepatocytes. Hepatology *51*, 1334–1344.

McCallum, H., Jones, M., Hawkins, C., Hamede, R., Lachish, S., Sinn, D.L., Beeton, N., and Lazenby, B. (2009). Transmission dynamics of Tasmanian devil facial tumor disease may lead to disease-induced extinction. Ecology *90*, 3379–3392.

Montero, J., Morales, A., Llacuna, L., Lluis, J.M., Terrones, O., Basañez, G., Antonsson, B., Prieto, J., García-Ruiz, C., Colell, A., and Fernández-Checa, J.C. (2008). Mitochondrial cholesterol contributes to chemotherapy resistance in hepatocellular carcinoma. Cancer Res. *68*, 5246–5256.

Murchison, E.P., Tovar, C., Hsu, A., Bender, H.S., Kheradpour, P., Rebbeck, C.A., Obendorf, D., Conlan, C., Bahlo, M., Blizzard, C.A., et al. (2010). The Tasmanian devil transcriptome reveals Schwann cell origins of a clonally transmissible cancer. Science *327*, 84–87.

Murchison, E.P., Schulz-Trieglaff, O.B., Ning, Z., Alexandrov, L.B., Bauer, M.J., Fu, B., Hims, M., Ding, Z., Ivakhno, S., Stewart, C., et al. (2012). Genome sequencing and analysis of the Tasmanian devil and its transmissible cancer. Cell *148*, 780–791.

Mutemberezi, V., Guillemot-Legris, O., and Muccioli, G.G. (2016). Oxysterols: From cholesterol metabolites to key mediators. Prog. Lipid Res. *64*, 152–169.

Nielsen, S.F., Nordestgaard, B.G., and Bojesen, S.E. (2012). Statin use and reduced cancer-related mortality. N. Engl. J. Med. *367*, 1792–1802.

Parton, R.G., and del Pozo, M.A. (2013). Caveolae as plasma membrane sensors, protectors and organizers. Nat. Rev. Mol. Cell Biol. *14*, 98–112.

Patchett, A.L., Darby, J.M., Tovar, C., Lyons, A.B., and Woods, G.M. (2016). The immunomodulatory small molecule imiquimod induces apoptosis in devil facial tumour cell lines. PLoS ONE *11*, e0168068.

Pearse, A.-M., and Swift, K. (2006). Allograft theory: transmission of devil facial-tumour disease. Nature *439*, 549.

Peet, D.J., Turley, S.D., Ma, W., Janowski, B.A., Lobaccaro, J.M., Hammer, R.E., and Mangelsdorf, D.J. (1998). Cholesterol and bile acid metabolism are impaired in mice lacking the nuclear oxysterol receptor LXR alpha. Cell *93*, 693–704.

Pelton, K., Coticchia, C.M., Curatolo, A.S., Schaffner, C.P., Zurakowski, D., Solomon, K.R., and Moses, M.A. (2014). Hypercholesterolemia induces angiogenesis and accelerates growth of breast tumors *in vivo*. Am. J. Pathol. *184*, 2099–2110.

Phalen, D.N., Frimberger, A., Pyecroft, S., Peck, S., Harmsen, C., Lola, S., de Mello Mattos, B., Li, K.M., McLachlan, A.J., and Moore, A. (2013). Vincristine chemotherapy trials and pharmacokinetics in Tasmanian devils with Tasmanian devil facial tumor disease. PLoS ONE *8*, e65133.

Phalen, D.N., Frimberger, A.E., Peck, S., Pyecroft, S., Harmsen, C., Lola, S., and Moore, A.S. (2015). Doxorubicin and carboplatin trials in Tasmanian devils (*Sarcophilus harrisii*) with Tasmanian devil facial tumor disease. Vet. J. *206*, 312–316.

Pommier, A.J., Alves, G., Viennois, E., Bernard, S., Communal, Y., Sion, B., Marceau, G., Damon, C., Mouzat, K., Caira, F., et al. (2010). Liver X Receptor activation downregulates AKT survival signaling in lipid rafts and induces apoptosis of prostate cancer cells. Oncogene *29*, 2712–2723.

Prêtre, V., and Wicki, A. (2018). Inhibition of Akt and other AGC kinases: A target for clinical cancer therapy? Semin. Cancer Biol. *48*, 70–77.

Pyecroft, S.B., Pearse, A.-M., Loh, R., Swift, K., Belov, K., Fox, N., Noonan, E., Hayes, D., Hyatt, A.D., Wang, L.F., et al. (2007). Towards a case definition for Devil Facial Tumour Disease: What is it? EcoHealth *4*, 346–351.

Raez, L.E., Papadopoulos, K., Ricart, A.D., Chiorean, E.G., Dipaola, R.S., Stein, M.N., Rocha Lima, C.M., Schlesselman, J.J., Tolba, K., Langmuir, V.K., et al. (2013). A phase I dose-escalation trial of 2-deoxy-D-glucose alone or combined with docetaxel in patients with advanced solid tumors. Cancer Chemother. Pharmacol. *71*, 523–530.

Rao, S., Lowe, M., Herliczek, T.W., and Keyomarsi, K. (1998). Lovastatin mediated G1 arrest in normal and tumor breast cells is through inhibition of CDK2 activity and redistribution of p21 and p27, independent of p53. Oncogene *17*, 2393–2402.

Repa, J.J., and Mangelsdorf, D.J. (2000). The role of orphan nuclear receptors in the regulation of cholesterol homeostasis. Annu. Rev. Cell Dev. Biol. *16*, 459–481.

Repa, J.J., and Mangelsdorf, D.J. (2002). The liver X receptor gene team: potential new players in atherosclerosis. Nat. Med. *8*, 1243–1248.

Rothblat, G.H., de la Llera-Moya, M., Atger, V., Kellner-Weibel, G., Williams, D.L., and Phillips, M.C. (1999). Cell cholesterol efflux: integration of old and new observations provides new insights. J. Lipid Res. *40*, 781–796.

Russell, D.W. (2000). Oxysterol biosynthetic enzymes. Biochim. Biophys. Acta *1529*, 126–135.

Schoonjans, K., Annicotte, J.S., Huby, T., Botrugno, O.A., Fayard, E., Ueda, Y., Chapman, J., and Auwerx, J. (2002). Liver receptor homolog 1 controls the expression of the scavenger receptor class B type I. EMBO Rep. *3*, 1181–1187.

Siddle, H.V., and Kaufman, J. (2013). How the devil facial tumor disease escapes host immune responses. OncoImmunology *2*, e25235.

Siddle, H.V., Kreiss, A., Tovar, C., Yuen, C.K., Cheng, Y., Belov, K., Swift, K., Pearse, A.-M., Hamede, R., Jones, M., et al. (2013). Reversible epigenetic down-regulation of MHC molecules by devil facial tumour disease illustrates immune escape by a contagious cancer. Proc. Natl. Acad. Sci. USA *110*, 5103–5108.

Silvente-Poirot, S., and Poirot, M. (2012). Cholesterol metabolism and cancer: the good, the bad and the ugly. Curr. Opin. Pharmacol. *12*, 673–676.

Simons, K., and Ikonen, E. (2000). How cells handle cholesterol. Science *290*, 1721–1726.

Simons, K., and Sampaio, J.L. (2011). Membrane organization and lipid rafts. Cold Spring Harb. Perspect. Biol. *3*, a004697.

Sorrentino, G., Ruggeri, N., Specchia, V., Cordenonsi, M., Mano, M., Dupont, S., Manfrin, A., Ingallina, E., Sommaggio, R., Piazza, S., et al. (2014). Metabolic control of YAP and TAZ by the mevalonate pathway. Nat. Cell Biol. *16*, 357–366.

Stammnitz, M.R., Coorens, T.H.H., Gori, K.C., Hayes, D., Fu, B., Wang, J., Martin-Herranz, D.E., Alexandrov, L.B., Baez-Ortega, A., Barthorpe, S., et al. (2018). The Origins and Vulnerabilities of Two Transmissible Cancers in Tasmanian Devils. Cancer Cell *33*, 607–619.e15.

Thupari, J.N., Pinn, M.L., and Kuhajda, F.P. (2001). Fatty acid synthase inhibition in human breast cancer cells leads to malonyl-CoA-induced inhibition of fatty acid oxidation and cytotoxicity. Biochem. Biophys. Res. Commun. *285*, 217–223.

Tsan, Y.T., Lee, C.H., Wang, J.D., and Chen, P.C. (2012). Statins and the risk of hepatocellular carcinoma in patients with hepatitis B virus infection. J. Clin. Oncol. *30*, 623–630.

Venkateswaran, A., Laffitte, B.A., Joseph, S.B., Mak, P.A., Wilpitz, D.C., Edwards, P.A., and Tontonoz, P. (2000). Control of cellular cholesterol efflux by the nuclear oxysterol receptor LXR alpha. Proc. Natl. Acad. Sci. USA *97*, 12097–12102.

Villa, G.R., Hulce, J.J., Zanca, C., Bi, J., Ikegami, S., Cahill, G.L., Gu, Y., Lum, K.M., Masui, K., Yang, H., et al. (2016). An LXR-Cholesterol Axis Creates a Metabolic Co-Dependency for Brain Cancers. Cancer Cell *30*, 683–693.

Wang, H.H., Afdhal, N.H., and Wang, D.Q. (2006). Overexpression of estrogen receptor alpha increases hepatic cholesterogenesis, leading to biliary hypersecretion in mice. J. Lipid Res. *47*, 778–786.

Wei, G., Twomey, D., Lamb, J., Schlis, K., Agarwal, J., Stam, R.W., Opferman, J.T., Sallan, S.E., den Boer, M.L., Pieters, R., et al. (2006). Gene expression-based chemical genomics identifies rapamycin as a modulator of MCL1 and glucocorticoid resistance. Cancer Cell *10*, 331–342.

Xu, Y., Li, F., Zalzala, M., Xu, J., Gonzalez, F.J., Adorini, L., Lee, Y.K., Yin, L., and Zhang, Y. (2016). Farnesoid X receptor activation increases reverse cholesterol transport by modulating bile acid composition and cholesterol absorption in mice. Hepatology *64*, 1072–1085.

Zelcer, N., Hong, C., Boyadjian, R., and Tontonoz, P. (2009). LXR regulates cholesterol uptake through Idol-dependent ubiquitination of the LDL receptor. Science *325*, 100–104.

Zhang, H., Temel, R.E., and Martel, C. (2014). Cholesterol and lipoprotein metabolism: Early Career Committee contribution. Arterioscler. Thromb. Vasc. Biol. *34*, 1791–1794.

Zheng, X., Cui, X.X., Gao, Z., Zhao, Y., Lin, Y., Shih, W.J., Huang, M.T., Liu, Y., Rabson, A., Reddy, B., et al. (2010). Atorvastatin and celecoxib in combination inhibits the progression of androgen-dependent LNCaP xenograft prostate tumors to androgen independence. Cancer Prev. Res. (Phila.) *3*, 114–124.

STAR★METHODS

KEY RESOURCES TABLE

REAGENT or RESOURCE	SOURCE	IDENTIFIER
Antibodies		
Total AKT	Cell signaling	Cat#4685; AB_2225340
Phosphorylated AKT Serine-473	Cell signaling	Cat #4060; AB_2797780
Phosphorylated AKT Threonine-308	Cell signaling	Cat #4056; AB_331163
Donkey Anti-Mouse IgG Antibody, HRP conjugate,	Sigma-Aldrich	Cat#AP192P
HRP-conjugated Anti-Rabbit IgG Concentrate	Sigma-Aldrich	Cat#RABHRP1
Anti-actin	Proteintech	Cat# 60008-1
Chemicals, peptides, and recombinant proteins		
β-methyl-cyclodextrin	Sigma-Aldrich	C4555
Water-soluble cholesterol	Sigma-Aldrich	C4951
U18666A	Cayman Chemicals	10009085; CAS: 3039-71-2
Atorvastatin	Sigma-Aldrich	Y0002229
Ly294002	Sigma-Aldrich	L9908
C75	Cayman Chemicals	9000783; CAS: 1234694-20-2
TOFA	Cayman Chemicals	10005263; CAS: 54857-86-2
2-Deoxyglucose	Sigma-Aldrich	D8375
T0901317	Cayman Chemicals	71810; CAS: 293754-55-9
Fulvestrant	Cayman Chemicals	10011269; CAS: 129453-61-8
Aicar	Cayman Chemicals	10010241; CAS: 3031-95-6
Metformin	Cayman Chemicals	13118; CAS: 1115-70-4
EX527	Cayman Chemicals	10009798; CAS: 49843-98-3
GW4064	Cayman Chemicals	10006611; CAS: 278779-30-9
Wy14643	Cayman Chemicals	70730; CAS: 50892-23-4
H-89	Cayman Chemicals	10010556; CAS: 130964-39-5
ML265	Cayman Chemicals	13942; CAS: 1221186-53-3
NSC23766	Cayman Chemicals	13196; CAS: 1177865-17-6
AZD8055	Cayman Chemicals	16978; CAS: 1009298-09-2
GDC-0068	Cayman Chemicals	18412; CAS: 1001264-89-6
MK2206	Cayman Chemicals	11593; CAS: 1032350-13-2
Rapamycin	Cayman Chemicals	13346; CAS: 53123-88-9
8-Bromo-cyclic AMP (8Br-cAMP)	Cayman Chemicals	14431; CAS: 76939-46-3
DLPC	Cayman Chemicals	11023; CAS: 18194-25-7
NSC23766	Cayman Chemicals	13196; CAS: 1177865-17-6
Nicotinamide (NAM)	Sigma-Aldrich	N0636; CAS: 98-92-0
Clostridium botulinum ADP-ribosyltransferase C3	Cytoskeleton, Inc	CT03
Carboxy-H_2DCFDA	Invitrogen	C400
24(S)-Hydroxycholesterol (24-OHC)	Avanti Polar Lipids	700071P: CAS: 474-73-7
25(S)-Hydroxycholesterol (25-OHC)	Avanti Polar Lipids	700019P: CAS: 2140-46-7
27(S)-Hydroxycholesterol (27-OHC)	Avanti Polar Lipids	700021P: CAS: 20380-11-4
PitStop2	Abcam	AB120687: CAS: 1419093-54-1
Dyngo	Abcam	AB120689: CAS: 1256493-34-1

(*Continued on next page*)

Continued

REAGENT or RESOURCE	SOURCE	IDENTIFIER
Propidium iodide (PI)	Sigma-Aldrich	P4170; CAS: 25535-16-4
DMSO	Sigma-Aldrich	D8418; CAS: 67-68-5
Ultraglutamine	LONZA	H3BE17-605E/U1
AmnioMAXTM-C100 (1X) Basal Medium	Invitrogen	17001082
Glucose	Sigma-Aldrich	G8270; CAS: 50-99-7
Sodium Pyruvate Solution	LONZA	H3BE13-115E
Oligomycin	Agilent	103015-100; CAS: 579-13-5
Carbonyl cyanide-p-trifluoromethoxyphenylhydrazone (FCCP)	Agilent	103015-100; CAS: 370-86-5
Rotenone	Agilent	103015-100; CAS: 83-79-4
antimycin	Agilent	103015-100; CAS: 1397-94-0
Filipin III	Sigma-Aldrich	F4767; CAS: 480-49-9
LPDS	Sigma-Aldrich	LP4
Penicillin/streptomycin	Sigma-Aldrich	P4333
Sodium dodecyl sulfate	Sigma-Aldrich	L3771; CAS: 151-21-3
L- Glutamine	Sigma-Aldrich	G3126; CAS: 56-85-9
Thiazolyl Blue Tetrazolium Bromide	Sigma-Aldrich	M2128; CAS: 206-069-5
Neon transfection buffer R	Invitrogen	Cat#MKP1025
Cas9	Invitrogen	Cat#A36498
Protease Inhibitors	Roche Diagnostics	COEDTAF-RO
Phosphatase Inhibitors cocktail	Roche Diagnostics	P2850
Rhodamine 123	Sigma-Aldrich	R8004; CAS: 62669-70-9
Critical commercial assays		
Annexin V-FITC Apoptosis detection kit	BD Biosciences	Cat#556547
Amplex® Red Hydrogen Peroxidase assay kit	Molecular Probes, Invitrogen	Cat#A22188
Amplex® Red Cholesterol Assay Kit	Molecular Probes, Invitrogen	Cat#A12216
SensiFAST kit	Bioline	Cat#BIO-65054
Pierce ECL Western Blotting Substrate kit	Pierce	Cat#34095
Seahorse XF Cell Mito Stress kit	Agilent	Cat#103015-100
Deposited data		
Raw data western-blots	Mendeley	10.17632/44ky4hzhcw.1
Experimental models: cell lines		
DFTD1	Department of Primary Industries, Parks, Water and Environment (DPIPWE), State Government of Tasmania, Australia	N/A
DFTD2	Department of Primary Industries, Parks, Water and Environment (DPIPWE), State Government of Tasmania, Australia	N/A
DFTD4	Department of Primary Industries, Parks, Water and Environment (DPIPWE), State Government of Tasmania, Australia	N/A
FIBS	Department of Primary Industries, Parks, Water and Environment (DPIPWE), State Government of Tasmania, Australia	N/A
Experimental models: organisms/strains		
Nude mice	Australian Resources Centre	BALB/c-Foxn1^{nu}/Arc
Oligonucleotides		
Alt-R CRISPR Cas9 sgRNA AKT1 5′-GGCCACAAGATGTGGACCAG-3′	IDT	N/A

(*Continued on next page*)

Continued

REAGENT or RESOURCE	SOURCE	IDENTIFIER
Alt-R CRISPR Cas9 sgRNA AKT3 5′-TATAGAACGAACATTTCATG-3′	IDT	N/A
Alt-R CRISPR Cas9 sgRNA LXRb 5′-GCGGCGCTACAACCACGAGA-3′	IDT	N/A
18S Forward 5′-AGCGGCTGAAGAAGATACGG -3′	IDT	N/A
18S Reverse 5′-TTGGACACACCCACAGTACG -3′	IDT	N/A
Actin Forward 5′-TGTGCGACGAAGACGAGAC -3′	IDT	N/A
Actin Reverse 5′-GACCCATACCCACCATGACG -3′	IDT	N/A
ABCG1 Forward 5′-AGACCATGGCTGATGTTCCC -3′	IDT	N/A
ABCG1 Reverse 5′-AGAGACTGAGCCACCAGTGA -3′	IDT	N/A
FASN Forward 5′-CGCTGTCCCAAGGGTATTGT -3′	IDT	N/A
FASN Reverse 5′-GCAAATACCCCCTCAGCCTT -3′	IDT	N/A
SREBP1c (SREBP) Forward 5′-GGCGGGGCTACACCTGCCTTCCA -3′	IDT	N/A
SREBP1c (SREBP) Reverse 5′-ACCAGCCCCCTCCTCCTCCTCCT -3′	IDT	N/A
HMG-CoA-REDUCTASE Forward 5′-GCCTGTTCCTGTTGGAGTAGCAGGGC -3′	IDT	N/A
HMG-CoA-REDUCTASE Reverse 5′-ACAGCCTTCAGTGGTGGCCATAGGGA -3′	IDT	N/A
ABCG8 Forward 5′-AGAAGGTCAAGTCCCTCGCTGCCTTGT -3′	IDT	N/A
ABCG8 Reverse 5′-TCGGGCATCTGCCTCCAAGAAGCAACT -3′	IDT	N/A
Software and algorithms		
ADOBE Photoshop CC3	ADOBE	N/A
FlowJo (LCC Ashland, Oregon, US)	FlowJo, LCC Ashland, Oregon, US	N/A
LAS V413 Fluorescence software	Leica	N/A
GraphPad Software, Inc version 8	GraphPad	N/A
ImageJ	NIH	N/A
Other		
Leica DMIL LED epifluorescence microscope	Leica	N/A
Neon Transfection System	Invitrogen	Cat#MKP5000
BD LSR Fortessa 5 analyzer	BD Biosciences	N/A
BD fluorescence-activated cell sorter (FACS) Canto II	BD Biosciences	N/A
Microplate reader BIOTEK PowerWave XS	Biotek	N/A
Seahorse XFe96 analyzer	Agilent	N/A
ZOE Fluorescent Cell Imager	BioRad	N/A

RESOURCE AVAILABILITY

Lead contact

Further information and requests for resources and reagents should be directed to and will be fulfilled by the lead contact, Manuel A. Fernandez-Rojo (manuel.fernandez@imdea.org).

Materials availability

All unique reagents generated in this study are available from the lead contact with a completed Materials Transfer Agreement and after separate agreements with DPIPWE and the State of Tasmania.

Data and code availability

Raw data regarding western blots in this manuscript have been deposited in Mendeley under the reference 10.17632/44ky4hzhcw.1

EXPERIMENTAL MODEL AND SUBJECT DETAILS

Animal studies

Ten females seven-week old BALB/c nude mice were maintained with *ad libitum* food and water availability and standard housing guidelines at the QIMR Berghofer Institute. The mice were injected subcutaneously (*s.c.*) with approx. 6×10^6 DFTD4 cells in both flanks to develop two tumors per mouse. Four-five weeks later, when the tumors were at palpable size, we initiated treatment with atorvastatin (10 mg/kg/mouse). Briefly, mice were divided in two groups of five, that corresponded to ten tumors per group (i.e., two tumors per mouse), which were treated with vehicle (PBS) or atorvastatin. Every two days and for a total of twelve days, mice were injected intraperitoneal *(i.p.)* with either atorvastatin or PBS in a final volume of 100 μl. We assessed the impact of atorvastatin on tumor growth as previously described (Ikonomopoulou et al., 2018). The concentration chosen for atorvastatin is reported in the literature to be innocuous when administered at 10mg/kg daily for 42 days by i.p. in nude mice (Zheng et al., 2010). The effects of atorvastatin on tumor progression were estimated by calculating the fold-change in size versus the initial size prior to the first injection of atorvastatin (day 0). At the end of the experiment, mice were euthanised with CO_2 and tumors were harvested for histology (Hematoxylin and Eosin staining). The animal experimental procedure was assessed and approved by the QIMR Berghofer MRI Institute's ethics committee (Project number: P2290 and ethics committee approval number: A1703-603M).

METHOD DETAILS

DFTD cell lines and cell culture

All DFTD (DFTD1, DFTD2 and DFTD4) and fibroblast (FIBS) cell lines were obtained from the Department of Primary Industries, Parks, Water and Environment (DPIPWE), State Government of Tasmania, Australia, and were established as part of a management plan and adhered to a standard operating practice. Information on the devil cell lines is provided in Fernandez-Rojo et al. (2018). Devil Facial Tumor cancer cell lines, and the control Tasmanian Devil fibroblast (FIBS) healthy cell line were maintained in a humidified incubator at 35°C and 5% CO_2. The DFTD strains were cultured in RPMI-1640 media that was supplemented with 10% FCS, and 2mM Glutamax™. The FIBS was grown in GIBCO AmnioMAX-C100 Basal Medium liquid, containing AmnioMAX-C100 Supplement. Penicillin/streptomycin (PS) (100U/ml each) was added in all media. Cells were passaged at approximately 90% confluency. Functional studies were performed with passages up to 20. All cell lines were mycoplasma free (QIMR Berghofer, Scientific Services, AU).

Cell viability

Cell viability was measured by MTT as previously described (Fernandez-Rojo et al., 2018). In brief, 8000 (DFTD) and 5,000 (FIBS) cells/well were seeded in a 96-flat adherent microtiter well plate for 24 h to allow cell adhesion. MCD, cholesterol, U18666A, atorvastatin or other drugs were then added and MTT reduction was measured after 48 h at 540 nm absorbance in a microplate reader (BIOTEK PowerWave XS). 0.1% Sodium dodecyl sulfate (SDS) was used as a positive control (100% toxicity). A row of untreated cells was used to define 100% viability and blank wells containing only media were used to extract background. The concentration of MCD, cholesterol, U18666A or atorvastatin causing 50% inhibition (EC_{50}) in DFTD and FIBS cells was determined using GraphPad Software, Inc (US).

Seahorse glycolysis and mitochondrial respiration flux analysis

To measure key parameters of mitochondrial function by measuring the oxygen consumption rate (OCR), we seeded 4×10^4 and $2 \cdot x$ 10^4 cell/well in 100 μL of DFTD and FIBS cells respectively, in a XF96 Cell Culture Microplates pre-coated with collagen (0.9mg/ml). 24 hours later, the cells (four wells/treatment/replicate) were exposed to TO901317 (1μM), 24-OHC (10μM) or atorvastatin (15μM) in 100 μL/well RPMI 1640 with Ultraglutamine 1 and 25 mM HEPES media (Lonza) in case of the DFTD cells and 100 μL/well AmnioMAXTM-C100 (1X) Basal Medium in case of the FIBS cells.

The following day, the existent media was replaced by 180 μL/well Seahorse XF base medium (pH 7.4) with 15 mM Glucose, 1 mM Pyruvate, 2 mM Glutamine, and the corresponding concentrations of each treatment (Control DMSO (0.001% (v/v)); Control

Methanol (0.004% (v/v)); Atorvastatin (15 μM); T090 (1 μM); 24 OHC (10 μM)) and cells were further incubated into a 37°C non-CO_2 incubator for 1 hour. Meanwhile, injections were prepared using the Seahorse XF base medium supplemented as detailed above and 2 μM Oligomycin (port A), 0.3 μM carbonyl cyanide-p-trifluoromethoxyphenylhydrazone (FCCP, port B) and 0.5 μM Rotenone/antimycin (port C) (final well concentration). Then, the plate and the cartridge were placed in the Seahorse XFe96 analyzer where the cycles of measurement involved 3 min mixing, 3 min waiting and 3 min measuring prior to the first injection and also after each injection. The measurement data were analyzed following the Seahorse XF Cell Mito Stress Test Equations & Example Calculations.

To test glycolytic function in cells by directly measuring the extracellular acidification rate (ECAR), both type of cells, DFTD and FIBS, were seeded and treated as to measure OCR. The day of the analysis, the existent media was replaced by 180 μL/well Seahorse XF base medium (pH 7.4) supplemented with 0.5 mM Pyruvate, 1 mM Glutamine and the corresponding concentrations of each treatment (Control DMSO (0.001% (v/v)); Control Methanol (0.004% (v/v)); Atorvastatin (15 μM); T090 (1 μM); 24 OHC (10 μM)) The cell culture microplate was placed into a 37°C non-CO_2 incubator for 1 h. The injections were prepared using the detailed medium and 10 mM Glucose (port A), 1 μM Oligomycin (port B) and 50 mM 2-Deoxy-D-glucose (2-DG, port C) (final well concentration). The measurements were executed and analyzed in the same way as in the OCR analysis. For both assays, each treatment was replicated in 4 wells and 3 to 5 complete assays were performed.

Filipin staining

DFTD4 cells in glass coverslips were fixed in PFA 4% for 1 hour, followed by three washes in PBS, then incubated in Filipin solution (1/500 dilution in PBS from a stock of 10 μg/ml) for 30 minutes. Afterward, coverslips were washed in PBS and set in glass slides. Images were taken using Leica DMIL LED epifluorescence microscope and using the LAS V413 Fluorescence software. Panel figures were set using ADOBE photoshop.

Knockout of LXRβ, AKT1 and AKT3 in DFTD4 cells

For CRISPR-Cas9 targeting of DFTD4 cells the following sgRNA sequences were ordered from IDT (Alt-R CRISPR Cas9 sgRNA): AKT1 5′-GGCCACAAGATGTGGACCAG-3′, AKT3 5′-TATAGAACGAACATTTCATG-3′, LXRb 5′-GCGGCGCTACAACCACGAGA-3′. For RNP complex formation, 2.5 μg Cas9 (Invitrogen, #A36498) and 2 μg of each sgRNA were incubated for 5min at 37°C in 10 μL Neon transfection buffer R (Invitrogen, #MKP1025). 2 × 10^5 DFTD4 cells were resuspended in RNP transfection mix and electroporated using the Neon Transfection System (Invitrogen, #MKP5000) under the following conditions: Voltage = 1500, Pulse width = 20, Pulse numbers = 2. Cells were placed in warm media immediately after electroporation. When cells were sufficiently confluent, genomic DNA was extracted to assess InDel formation using Next Generation Sequencing analysis. Cells were observed for their proliferative potential alongside parental DFTD4 cells. For imaging of the DFTD we used the ZOE Fluorescent Cell Imager from Bio-Rad and captured images under bright field. The scale bar in each image is 50 microns.

Western blots

DFTD4 cells were lysed in cold RIPA buffer containing protease (Merck Pty Ltd, Kilsyth, Australia) and phosphatase (Roche Diagnostics, Castle Hill, Australia) inhibitors and stored at −20°C. Protein concentrations were determined using a Pierce BCA Protein assay kit (Thermo Fisher Scientific). Samples were subjected to SDS-PAGE and blotted according to standard procedures. In brief, 10 μg of protein was loaded per lane. Antibodies used for western blots are Phosphorylated AKT Threonine-308, Phosphorylated AKT Serine-473 and Total AKT (Cell signaling) and HRP-secondary antibodies (Sigma). Protein signals were visualized using enhanced chemiluminescence (Pierce ECL Western Blotting Substrate).

Cell cycle

DFTD4 cells were synchronized by removing serum from the media for ~24 h. Complete media was then added into cells treated with MCD, cholesterol, U18666A or atorvastatin for 24 hours. Cell cycle protocol is described in detail in Fernandez-Rojo et al. (2018). Cell pellets that were stained with 10 μl of propidium iodide (PI) (1 mg/ml) were analyzed at a maximum emission of 605 nm by BD LSR Fortessa 5 analyzer (BD Biosciences). Approximately 10,000 events were recorded, and data were analyzed using FlowJo software v10.06 (FlowJo, LCC Ashland, Oregon, US).

Cell apoptosis

Apoptosis in DFTD4 cells treated with MCD, cholesterol, U18666A or atorvastatin were measured by the BD fluorescence-activated cell sorter (FACS) Canto II high throughput system (HTS, BD Biosciences, San Diego, CA) using the Annexin V-FITC Apoptosis detection kit as previously described in Fernandez-Rojo et al. (2018). Briefly, cells were seeded at a density of ~100,000 in a round-bottom 96-well plate and treated with MCD, cholesterol, U18666A or atorvastatin for 24 hours. Cells were stained simultaneously with FITC-labeled annexin V and propidium iodide (PI) for 30 minutes in the dark and at room temperature before been analyzed using FlowJo software v10.06 (FlowJo, LCC Ashland, Oregon, US).

Reactive oxygen species

Amplex® Red Hydrogen Peroxidase assay kit (Invitrogen, AU) was used to measure ROS generation due to MCD, cholesterol, U18666A, C75, TOFA, HG, HG+2DG, LG or atorvastatin-treated DFTD4 cells for 24 h as we previously described in Fernandez-Rojo et al. (2018).

Fluorescent cells were analyzed by BD FACSCalibur flow cytometer (BD Biosciences, San Diego, CA) using an excitation and emission wavelength at 492 nm and 517 nm, respectively. The obtained data were analyzed using FlowJo (LCC Ashland, Oregon, US).

Mitochondria membrane potential

We measured mitochondria membrane potential (MMP) using Rhodamine 123 (Rhod-123), a cationic dye that is localized in mitochondria to assess the effect of MCD, cholesterol, U18666A or atorvastatin after 24 h of exposure as previously described (Fernandez-Rojo et al., 2018) and by flow cytometry (BD Biosciences, San Diego, CA, US). Data were analyzed using FlowJo (LCC Ashland, Oregon, US).

Real time PCR

Total RNA was isolated from both control and treated DFTD4 cells by using an RNeasy kit (QIAGEN, #74106) and cDNA synthesis was performed using SensiFAST kit (Bioline) according to manufacturerś protocol. Quantitative real-time PCR was completed using an Applied Biosystems 7900HT Fast Real-Time PCR System. For analyses, the gene expression levels were normalized to the mRNA expression levels of Tasmanian devil 18S used as housekeeping gene. All primers used in this manuscript are listed in the key resources table.

Measurement of the cholesterol content

Cholesterol content was measured in cell lysates of control (DMSO) and 24 hours treated (T0901317) cells using the Amplex® Red Cholesterol Assay Kit (Molecular Probes, Invitrogen), according to the manufacturer's instructions. The results were normalized to total cellular protein which was quantified using a BCA kit and following the manufacturerś guidelines.

QUANTIFICATION AND STATISTICAL ANALYSIS

In the viability experiments, we used One-Way ANOVA to assess differences due to drugs at various concentrations as well as permutation test for changes between DFTD versus FIBS in dose response experiments. To examine for changes among cell cycle phases, and if the data were normally distributed (i.e., Shapiro-Wilk or Kolmogorov-Smirnov test to examine normality), we used One-Way ANOVA. HG, HG+2DG, LG; PreG0 and G0/G1 phases were not normally distributed and neither were the PreGo phases for MCD, Chol and U18666. Thus, for these comparisons we used the non-parametric Kruskal-Wallis test. Changes in cell cycle phases due to atorvastatin treatment were examined by an unpaired t test. We used One-Way ANOVA to assess alterations among % of cell populations (i.e., healthy, early apoptotic, late apoptotic or necrotic) due to MCD, cholesterol and U18666A as well as unpaired t test for changes due to atorvastatin. ROS levels for HG and HG+2DG were examined by an unpaired t test while HG with LG by the nonparametric Mann-Whitney test. In addition, ROS changes for MCD and U1866 as well as control versus C75 treated cells were assessed by One-Way ANOVA. Variations caused by Cholesterol or TOFA were determined via the nonparametric Mann-Whitney test. The impact of atorvastatin on ROS was examined by an unpaired t test. One-way ANOVA was used to assess discrepancies for the mitochondrial membrane potential between MCD and cholesterol in response to control cells and Mann-Whitney nonparametric test for differences between control and U18666 treated cells as well as control and atorvastatin. In addition, we assessed differences from the seahorse experimental parameters, the alterations in gene expression levels and cholesterol content changes by unpaired t tests. The data are shown as the mean ± standard error. *$p < 0.05$, **$p < 0.01$, ***$p < 0.001$, ****$p < 0.0001$ are considered statistical significance. All experiments are the results of at least three independent experiments with three replicates each unless indicated otherwise. The average data of the experiments (e.g., cell cycle, ROS, MMP and apoptosis) are given in Tables S2–S5. Note that more statistical details and outcomes are provided in the appropriate result section and the figure legends. Finally, for the Animal Studies, we used the permutation test to evaluate differences in the tumor progression between atorvastatin-treated and vehicle-treated mouse groups for the duration of the experiment (*$p \leq 0.05$).

Cell Reports, Volume *34*

Supplemental information

LXR stimulates a metabolic switch and reveals cholesterol homeostasis as a statin target in Tasmanian devil facial tumor disease

Maria P. Ikonomopoulou, Yaiza Lopez-Mancheño, Marta G. Novelle, Maite Martinez-Uña, Lahiru Gangoda, Martin Pal, Luis Filipe Costa-Machado, Pablo Jose Fernandez-Marcos, Grant A. Ramm, and Manuel Alejandro Fernandez-Rojo

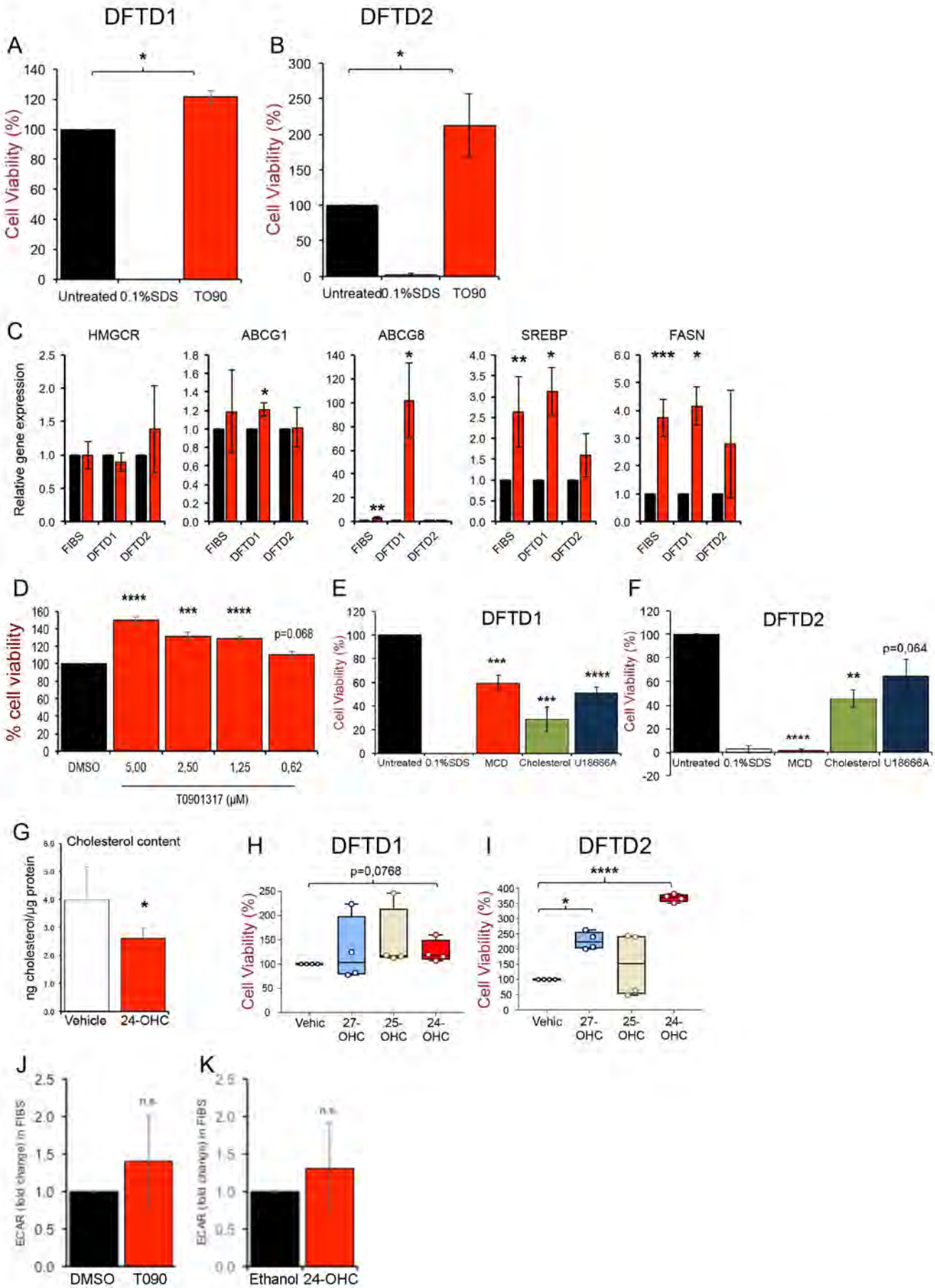
DFTD1
DFTD2
A
B
Cell Viability (%)
Untreated
0.1%SDS
TO90
C
HMGCR
ABCG1
ABCG8
SREBP
FASN
Relative gene expression
FIBS
DFTD1
DFTD2
D
% cell viability
DMSO
5,00
2,50
1,25
0,62
T0901317 (µM)
p=0.068
E
DFTD1
MCD
Cholesterol
U18666A
F
DFTD2
p=0,064
G
Cholesterol content
ng cholesterol/µg protein
Vehicle
24-OHC
H
DFTD1
p=0,0768
I
DFTD2
Vehic
27-OHC
25-OHC
24-OHC
J
ECAR (fold change) in FIBS
n.s.
DMSO
T090
K
Ethanol
24-OHC

Figure S1. LXR activation promotes DFTD proliferation as shown by MTT assay.
(A-B) **Related to figure 1 and 3.** The LXR agonist T0901317 (T090) stimulates cell proliferation in DFTD1 and DFTD2 cells. DMSO was used as the vehicle control and 0.1% sodium dodecyl sulphate (SDS) as the positive control, causing 100% toxicity. Four independent experiments were done in duplicates.
(C) Relative gene expression analysis of LXR-target genes in FIBS, DFTD1 and DFTD2 exposed to T0901317 (T090; 5μM, red bars) or vehicle control (DMSO) (black bars). Five independent experiments for FIBS and DFTD1 and three independent experiments for DFTD2 were performed.
(D) MTT proliferation assay assessing T0901317 at various concentrations in DFTD4 cells. Four independent experiments were done in duplicates.
(E-F) The treatment with MCD (0.05%), cholesterol (120μg/ml) or U18666A (7.5μM) for 48 hours reduced cell proliferation in (E) DFTD1 and (F) DFTD2 cells. DMSO was used as the vehicle control and 0.1% sodium dodecyl sulphate (SDS) as the positive control, causing 100% toxicity. Data are the result of four independent experiments in duplicates.
(G) Cholesterol content in 24-OHC (1μM) -treated DFTD4 cells in comparison to vehicle (ethanol). Five independent experiments were performed in duplicates.
(H-I) The effects on cell proliferation using the oxysterols 24-OHC, 25-OHC, 27-OHC versus untreated controls at 1μM in DFTD1 (H) and in DFTD 2 (I) cells. Four independent experiments were done in duplicates.
(J-K) Glycolytic flux (ECAR) in (J) T0931317 (T090)-treated and (K) 24OHC-treated FIBS cells in comparison to vehicle (DMSO and ethanol, respectively) represented as fold change of mpH/ mim. Five independent experiments were performed in five replicates.
Data are shown as mean ± SEM. Statistical analyses are relative to untreated cells and are represented as: *P<0.05, **P<0.01, ***P<0.001, ****P<0.0001.

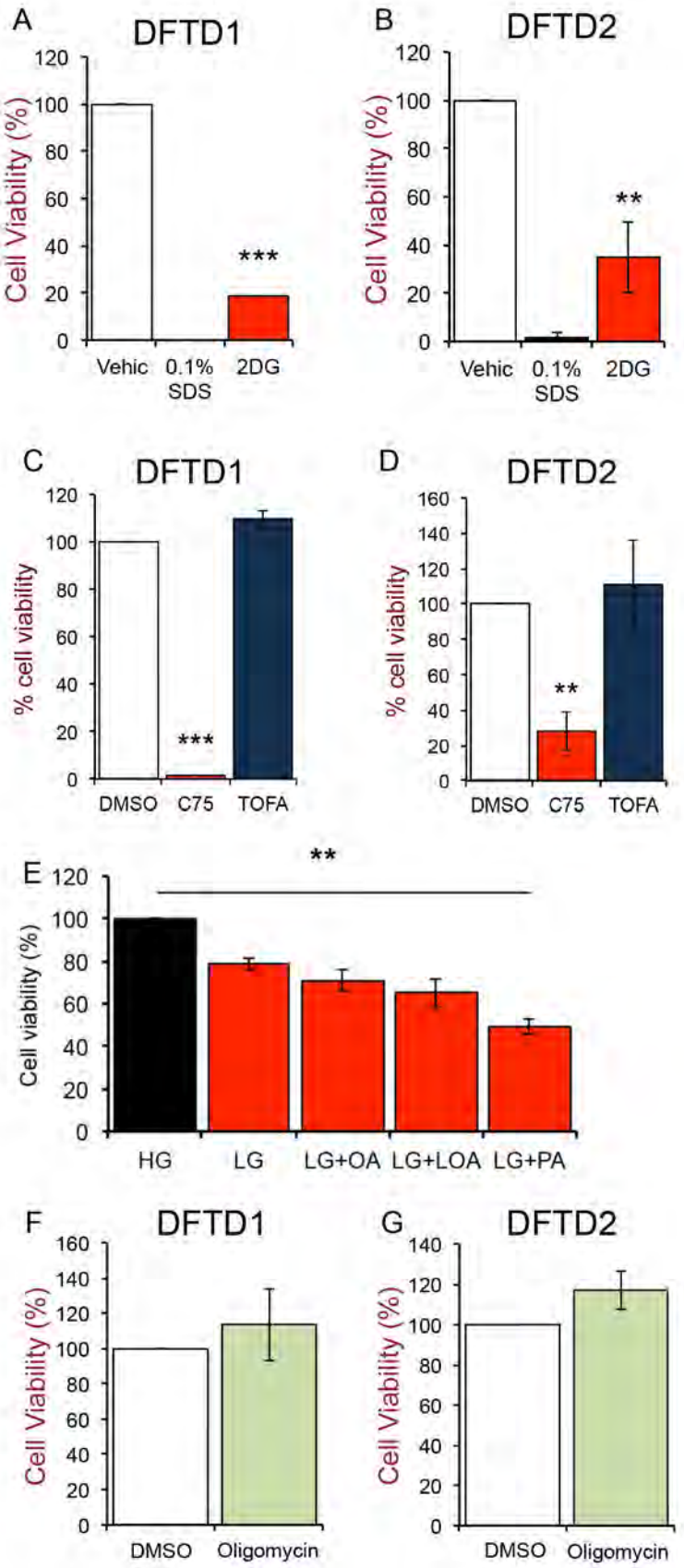
A
DFTD1
Cell Viability (%)
120
100
80
60
40
20
0
***
Vehic
0.1% SDS
2DG
B
DFTD2
Cell Viability (%)
**
Vehic
0.1% SDS
2DG
C
DFTD1
% cell viability
***
DMSO
C75
TOFA
D
DFTD2
% cell viability
160
140
**
DMSO
C75
TOFA
E
**
Cell viability (%)
HG
LG
LG+OA
LG+LOA
LG+PA
F
DFTD1
Cell Viability (%)
DMSO
Oligomycin
G
DFTD2
Cell Viability (%)
DMSO
Oligomycin

Figure S2. DFTD cells rely on aerobic glycolysis but not in lipogenesis and oxidative phosphorylation to proliferate. Related to figure 2.

Proliferation of DFTD1 and DFTD2 cells in response to (A-B) 2-DG (1mM) and
(C-D) C75 (1μM) and TOFA (1μM).

(E) Proliferation of DFTD4 cells in response to low-glucose (LG) medium, and LG supplemented with oleic acids (LG+OA), Linoleic and Oleic acid (LG+LOA) and Palmitic acid (LG+PA). The concentration of each fatty acid was 200μM. Data are the result of four independent experiments performed duplicates.

(F-G) Proliferation of DFTD1 and DFTD2 cells in response to Oligomycin (5μg/ml). 0.1% sodium dodecyl sulphate (SDS) was used as the positive control, causing 100% toxicity. Data are the result of an average of five independent experiments.

Data are shown as mean ± SEM. Statistical analyses are relative to untreated cells and are represented as: *P<0.05, **P<0.01, ***P<0.001, ****P<0.0001.

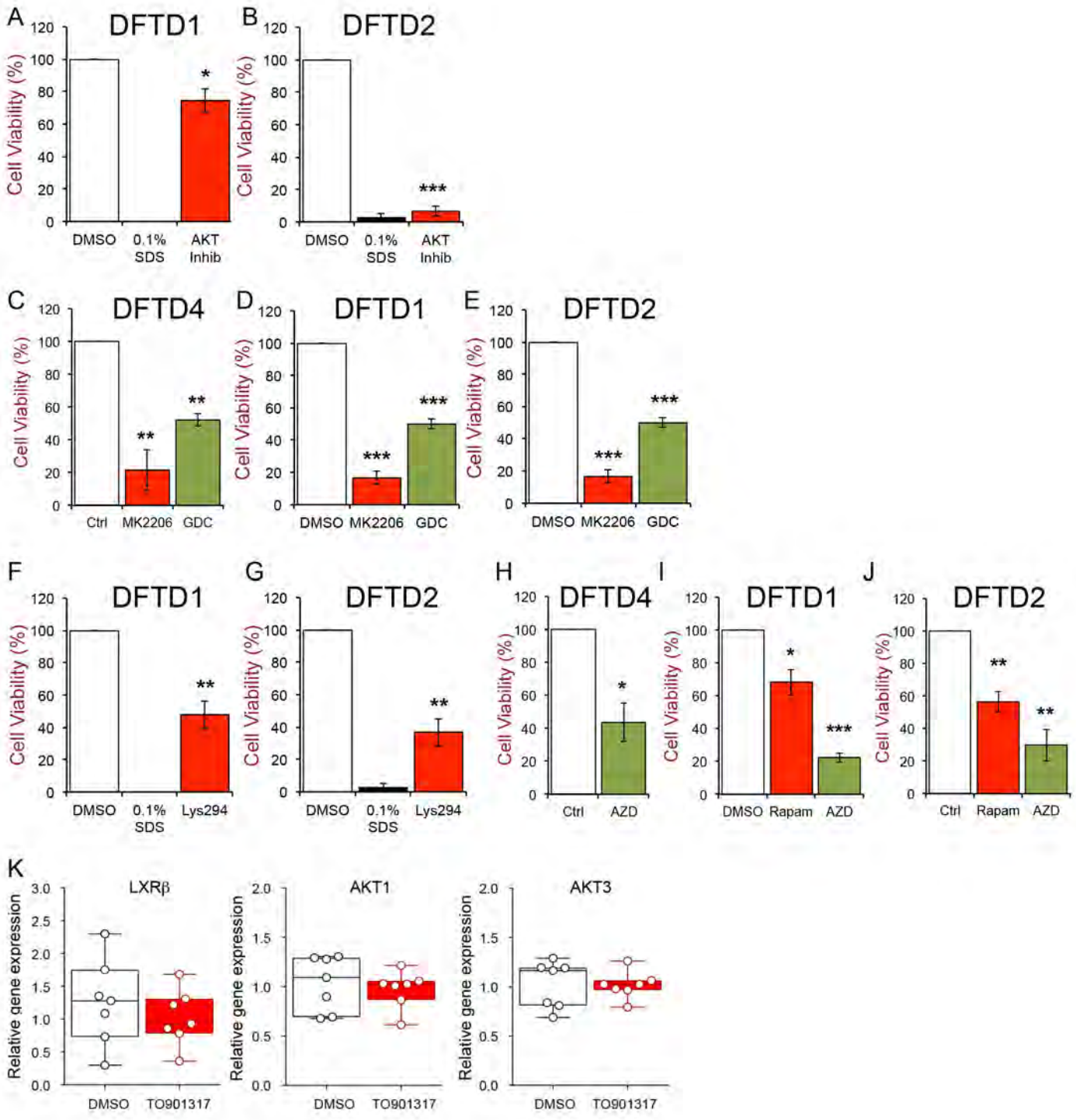
A
DFTD1
Cell Viability (%)
DMSO
0.1% SDS
AKT Inhib
B
DFTD2
C
DFTD4
Ctrl
MK2206
GDC
D
DFTD1
E
DFTD2
F
DFTD1
Lys294
G
DFTD2
H
DFTD4
AZD
I
DFTD1
Rapam
J
DFTD2
K
LXRβ
AKT1
AKT3
Relative gene expression
TO901317

Figure S3. Inhibition of the PI3K/AKT/mTOR signalling axis prevents DFTD growth. Related to figure 2. Cell proliferation assessment
(A-B) in DFTD1 and DFTD2 in response to AKT Inhibitor IX (1 μM);
(C-E). in DFTD4, DFTD1 and DFTD2 in response to AKT inhibitors MK2206 (10 μM) and GDC-0068 (1μM, GDC);
(F-G) in DFTD1 and DFTD2 in response to PI3K inhibitor LY294002 (30 μM, Lys294);
H in DFTD4 cells in response to the mTORC1 and mTORC2 inhibitor AZD8055 (1μM) and
(I-J) in DFTD1 and DFTD2 in response to Rapamycin (1 nM) and AZD8055 (1μM, AZD). 0.1% sodium dodecyl sulphate (SDS) as the positive control, causing 100% toxicity. Data are the result of an average of five independent experiments.
(K) Relative gene expression analysis of LXRβ, AKT1 and AKT3 in response to T0901317 or DMSO (as vehicle) in DFTD4 cells. Five independent experiments were performed.
Data are shown as mean ± SEM. Statistical analyses are relative to untreated cells and are represented as: *P<0.05, **P<0.01, ***P<0.001, ****P<0.0001.

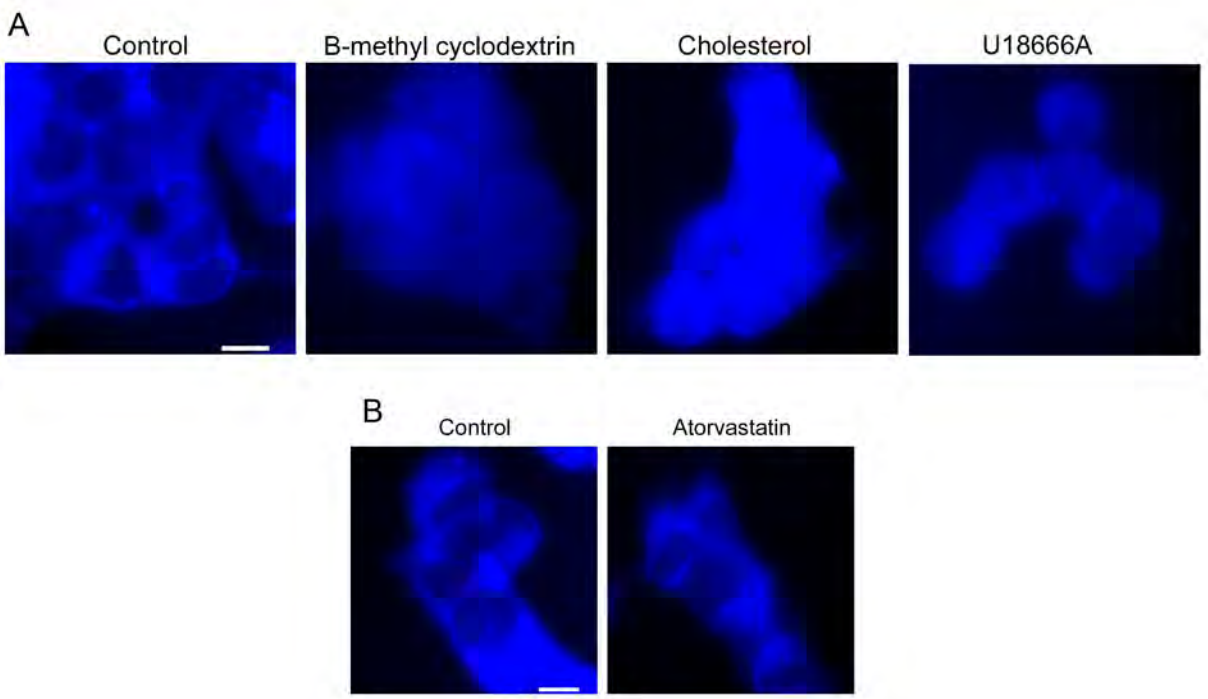
A
Control
B-methyl cyclodextrin
Cholesterol
U18666A
B
Control
Atorvastatin

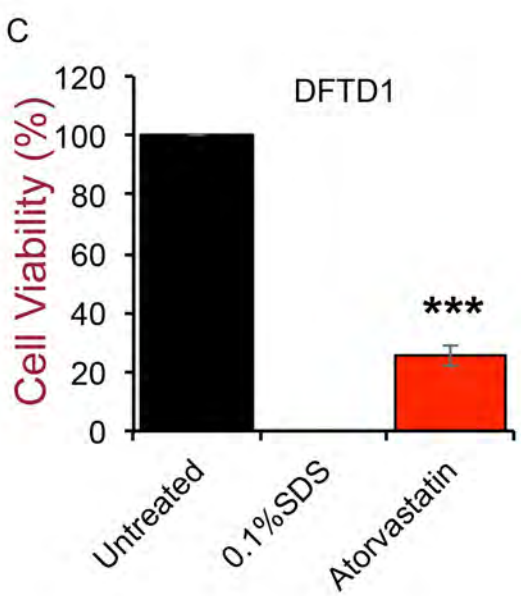
C
DFTD1
Cell Viability (%)
120
100
80
60
40
20
0
***
Untreated
0.1%SDS
Atorvastatin

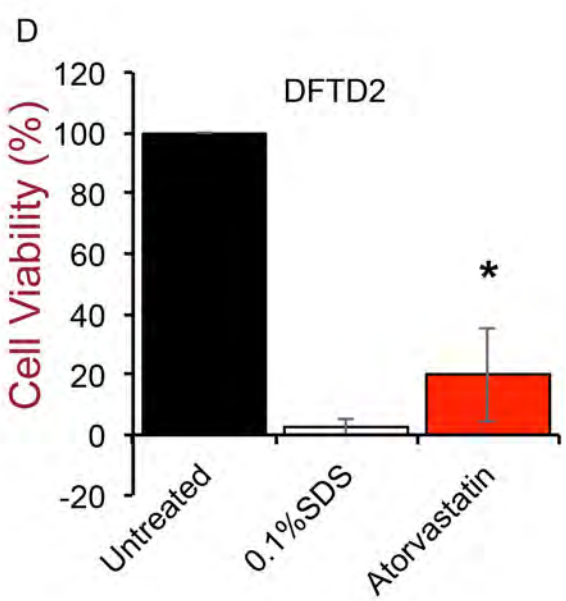
D
DFTD2
Cell Viability (%)
120
100
80
60
40
20
0
-20
*
Untreated
0.1%SDS
Atorvastatin

Figure S4. Atorvastatin inhibits DFTD cell proliferation. Related to figure 4. Filipin staining labelling cellular cholesterol in DFTD4 cells exposed to:
(A) MCD (0.05%), Cholesterol (120µg/ml) and U18666A (7µM) or
(B) Atorvastatin (15µM) for 24 hours. Scale bar: 100nm.
(C-D). Atorvastatin (15µM, 24 hours) reduces cell proliferation in DFTD1 and DFTD2 cells. DMSO was used as the vehicle control and 0.1% sodium dodecyl sulphate (SDS) as the positive control, causing 100% toxicity.
Data are shown as mean ± SEM. Data are the result of an average of five independent experiments performed duplicates. Statistical analyses are relative to untreated cells and are represented as: *P<0.05, **P<0.01, ***P<0.001, ****P<0.0001.

SUPPLEMENTAL MATERIAL.

Table S1. List of drugs tested in DFTD4 cells in the Figure 1b. Related to Figure 1.

Drug	PubChem ID	Concentration	Pathway	Target	Activity	References
Metformin	14219	1 mM	AMPK	Mitochondrial complex 1	Inhibitor	(Klein et al., 2004)
AICAR	17513	100 µM	AMPK	AMPK	Agonist	(Ayasolla et al., 2005)
PitStop2	136695100	7.5 µM	Endocytosis	Clathrin	Inhibitor	(von Kleist and Haucke, 2012)
Dyngo	72193863	5 µM	Endocytosis	Dynamin-2	Inhibitor	(McCluskey et al., 2013)
Nicotinamide (NAM)	936	5 mM	Deacetylation	Sirt-Family deacetylases	Inhibitor	(Dominguez-Gomez et al., 2015)
EX527	5113032	100 nM	Deacetylation	Sirt1	Inhibitor	(Gertz et al., 2013)
GW4064	9893571	3 µM	Nuclear receptors	FXRα	Agonist	(Xu et al., 2016)
T0901317	447912	5 µM	Nuclear receptors	LXR	Agonist	(Zelcer et al., 2009)
Wy14643	5694	5 µM	Nuclear receptors	PPARα	Agonist	(Fernandez-Rojo et al., 2013)
DLPC	512874	100 µM	Nuclear receptors	LRH-1	Agonist	(Schoonjans et al., 2002)
H-89	5702541	10 µM	PKA	PKA	Inhibitor	(Davies et al., 2000)
8-Bromo-cyclic AMP (8Br-cAMP)	23702958	50 µM	PKA	PKA	Agonist	(Sandberg et al., 1991)
Fulvestrant	17756771	1 µM	Estrogen receptor	Estrogen Receptor	Antagonist	(Wang et al., 2006)
ML265	404640608	10 µM	Actin cytoskeleton	PKM2	Inhibitor	(Palsson-McDermott et al., 2015)
C3-Transferase	318694076	1 µM	Actin cytoskeleton	Rho-1	Inhibitor	(Benink and Bement, 2005)
NSC23766	16759159	100 µM	Actin cytoskeleton	Rac1	Inhibitor	(Zhao et al., 2015)

Table S2. Average values of reactive oxygen species (ROS) caused in DFTD4 cells due to different treatments are given as ± SEM. Related to Figure 2, 3 and 4.

Treatment	**HG (Ctrl)**	**HG**	**HG+2DG**	**LG**
Values	4,82 ± 0.65	4,82 ± 0.65	0,95 ± 0,39	1,73 ± 0,87
Treatment	**Ctrl**	**C75**	**TOFA**	
Values	5,38 ± 1,07	22,63 ± 5,17	3,09 ± 1,35	
Treatment	**Ctrl**	**MCD**	**Cholesterol**	**U18666**
Values	4,8 ± 0,6	2,1 ± 0,4	3,4 ± 0,8	2,7 ± 1
Treatment	**DMSO (Ctrl)**	**Atorvastatin**	10,16 ± 2,78	18,76 ± 3,48
Values	4,27 ± 1,04	9,5 ± 3,3		

Table S3. Average values of the different cell cycle phases (PreG0, G0/G1, S & G2/M) due to various treatments in DFTD4 cells are given as ± SEM. Related to Figure 2, 3 and 4.

Cell Cycle phase	**PreG0**	**G0/G1**	**S**	**G2/M**
HG	3 ± 2,4	63,72 ± 11	9,80 ± 2,5	25,60 ± 3,5
HG+2DG	3,17 ± 4,95	63,35 ± 8,16	8,76 ± 2,4	24,97 ± 2,8
LG	2,67 ± 5,04	64,15 ± 3,5	10,93 ± 2,2	22,43 ± 2,7
Ctrl	10,4 ± 4,81	61,48 ± 5,06	9,82 ± 1,37	18,30 ± 2,43
MCD	5,75 ± 3,13	66,10 ± 3,42	6,74 ± 0,47	21,40 ± 1,29
Cholesterol	8,26 ± 4,32	62,20 ± 4,78	8,17 ± 1,28	21,38 ± 2,01
U18666	6,75 ± 4,69	63,78 ± 5,59	7,88 ± 1,86	21,50 ± 3,01
DMSO (Ctrl)	6,93 ± 2,76	61,72 ± 5,90	12,48 ± 2,09	18,82 ± 3,05
Atorvastatin	6,62 ± 4,57	64,46 ± 4,40	10,16 ± 2,78	18,76 ± 3,48

Table S4. Average values of cell populations (Healthy, early apoptotic, late apoptotic or necrotic) caused in DFTD4 cells due to different treatments are given as ± SEM. Related to Figure 2, 3 and 4.

	Healthy	**Early apoptotic**	**Late apoptotic**	**Necrotic**
Ctrl	55,97 ± 0,67	6,10 ± 1,95	17,47 ± 3,15	20,43 ± 5,31
MCD	58,13 ± 1,28	6,31 ± 2,39	22,50 ± 3,25	13,11 ± 4,38
Cholesterol	77,20 ± 6,50	1,71 ± 0,97	6,77 ± 3,43	14,36 ± 4,97
U18666	54,30 ± 4,0	9,87 ± 3,26	18,57 ± 7,28	21,50 ± 3,01
DMSO (Ctrl)	56,83 ± 3,03	6,02± 1,51	16,14 ± 4,68	17,30 ± 6,52
Atorvastatin	66,37 ± 0,33	12,49 ± 6,64	7,20 ± 0,94	21 ± 3,97

Table S5. Average values of mitochondrial membrane potential caused in DFTD4 cells due to different treatments are given as ± SEM. Related to Figure 3 and 4.

Control	MCD	Cholesterol	U18666		DMSO (Control)	Atorvastatin
64,28 ±10,80	57,72 ± 10,95	54,26 ± 11,91	62,10 ± 10,63		66,45 ± 6,87	68,42± 5,94